ORIGINAL PAPER

On bifurcations, resonances and dynamical behaviour in nonlinear iteroparous Leslie matrix models

Arild Wikan · Ørjan Kristensen

Abstract Leslie matrix models with nonzero nonlinear fecundity elements are under consideration. It is proved that by use of the general Deriso–Schnute recruitment function the supercritical nature of bifurcations in 2- and 3-age class models and a thorough analysis of 1:2 and 1:3 resonance phenomena are also provided. A discussion of impact of coexisting attractors and structures of trapping regions is included as well. Results regarding stabilizing and destabilizing effects as well as dynamical outcomes found in general n-age class models are also presented. Suggestions with respect to where our models may apply are provided too.

Keywords Leslie matrix models · Bifurcations · 1:2 and 1:3 resonance · Trapping region · Coexisting attractors · Complex dynamics

Mathematics Subject Classification code 37 · code 39

A. Wikan · Ø. Kristensen (✉)
School of Business and Economics, UiT The Arctic University of Norway, Havnegata 5, 9404 Harstad, Norway
e-mail: orjan.f.kristensen@uit.no

A. Wikan
e-mail: arild.wikan@uit.no

1 Introduction

If individuals of all age classes in an age-structured population are fertile, we say that the population possesses an iteroparous life history. In the case where individuals of the last age class only are fertile, the population is classified semelparous. Among several alternatives, nonlinear Leslie matrix models are widely used tools in order to capture and describe the dynamics as well as other properties of populations as described above. The usual approach in such models is to include nonlinearities (or density dependence) in fecundity terms and not in year-to-year survival probabilities. Particularly in fishery models [1], this has been motivated by the assumption that most density effects are present only in the first year of life. There are fewer studies where density dependence is incorporated in the survival or both in fecundity and survival terms, but see [2,3]. The dynamics obtained from semelparous and iteroparous population models are often very different. Regarding the semelparous case (nonlinear fecundities, constant survival probabilities), the nontrivial fixed point (equilibrium) tends to be unstable in most of the parameter space, and in contrast to what one finds from iteroparous models, also at low population densities. Instead, one observes a cyclic state where the whole population is in just one single-year class (SYC dynamics) at each time step, confer [4–11]. Ergodic properties of semelparous models may be obtained in [12,13], and in recent years we have seen much

attention towards describing and understanding insect cycles, in particular the 17 years cicada (magicicada) cycle, confer [14,15] and references therein. On the other hand, the dynamics found from Leslie matrix models where species who possess iteroparous life histories are targets, turns out to be quite different. Instead, by use of the compensatory Beverton and Holt recruitment function, the nontrivial fixed point was found to be stable in the whole parameter space, see [16–18]. However, in the overcompensatory Ricker case, the fixed point is stable at low population densities but the population may exhibit periodic, quasiperiodic as well as chaotic behaviour of stunning complexity at higher population densities, confer [19–27]. Regarding the work at hand, we shall use a much more sophisticated recruitment function than those referred to above, and thus, we will be able to show and prove several new and general results.

Let us now turn to 'real' populations. As it is well known, several fish populations of commercial interest, for example the Northeast Arctic cod stock may exhibit severe fluctuations in biomass from one year to another. In certain periods, the stock biomass seems to be dominated by strong year classes, while other periods show a more harmonic composition of the total stock biomass. Thus, by use of data from the fisheries, calibrated in order to fit, Leslie matrix models may provide important insight in complex dynamical behaviour and subsequently contribute to reliable fishing strategies.

Invading species may also become a serious problem. Both in the 1960s and the 1980s, pink salmon (also known as humpback salmon) was released in the Kola Peninsula in Russia. Later, the pink salmon has migrated to northern part of Norway, invaded rivers and represents today a severe threat to its Atlantic salmon rival, confer [28]. In 2021, local fish counts estimated up to 50,000 pink salmon in the Tana river (which is a famous 'salmon river' in northern Norway). Therefore, analysis of 2×2 Leslie matrix models (pink salmon) $n \times n$ models (Atlantic salmon) or a combination could provide valuable knowledge of dynamical behaviour and interaction, which again may be used in order to reduce and prevent the threat from the pink salmon.

Finally, as mentioned before, cicada cycles have on several occasions been studied by use of Leslie matrix models. Examples of insect species where such models could be excellent modelling tools may be found among caterpillars. Indeed, in recent years moth larvae have destroyed about 10,000 km^2 of birch forest in northern Scandinavia. Actually, there appears to be three different species responsible for the disaster, two species with high outbursts in numbers between 9 and 11 years, while the cycle is approximately 3 years for the last species. Climate warming is allowing these species to expand their ranges northwards, see [29]. Just as in the cicada case, discrete age-structured models could be very helpful in order to understand the mechanisms that lead to such outcomes.

Hence, in order to summarize, the more we know about the complex dynamics which nonlinear Leslie matrix models may generate, the better are our chances to describe and understand complicated dynamical phenomena that occur among species in nature.

The novelties of this paper are as follows: By use of a general recruitment function, we have been able to account for much more complex dynamical behaviour including births and deaths of coexisting attractors than in previous quoted papers. In another direction, we have presented proofs of nature of bifurcations involved both in 2- and 3-age class models as well as proofs of 1 : 2 and 1 : 3 resonance phenomena which lack in the literature. Regarding species who possess overcompensatory recruitment functions, the nonstationary dynamics of species of even and odd number of age classes differ in case of sufficiently large survival probabilities. We have also succeeded in finding an upper limit of population size where the population is stable in an n-age class model given that all survivals equal unity. At this limit, all eigenvalues of the linearized map are located on the boundary of the unit circle, which signals complex dynamical behaviour beyond instability threshold.

The plan of the paper is as follows: In Sect. 2, we present the model. Section 3 focuses on general properties, while we in Sects. 4 and 5 scrutinize 2- and 3-age class dynamics, respectively. Finally, in Sect. 6 we discuss and unify results obtained from general n-age class models, which is followed by a summary, Sect. 7.

2 The model

Let $x_{1,t}, \ldots, x_{n,t}$ be n nonoverlapping age classes of a population at time t and define the population vector $\overline{x}$ as $\overline{x} = (x_1, \ldots, x_n)^T$. Then we may express the relation between $\overline{x}$ at two consecutive time steps as a

map

$$h : \mathbb{R}^n \mapsto \mathbb{R}^n \quad \overline{x} \mapsto A\overline{x} \tag{1a}$$

or as a system of difference equations

$$\overline{x}_{t+1} = A\overline{x}_t \tag{1b}$$

where the $n \times n$ Leslie matrix A is defined as

$$A = \begin{pmatrix} f_1 & \cdots & f_{n-1} & f_n \\ p_1 & & 0 & 0 \\ & \ddots & & \vdots \\ 0 & & p_{n-1} & 0 \end{pmatrix} \tag{2}$$

Here f_i is the average fecundity (the number of daughters born per female in age class i), and p_i is the survival probability from age class i to age class $i + 1$.

The matrix elements may be density-dependent or not. In fishery models, one often assumes density-dependent fecundities and constant year-to-year survival probabilities. Moreover, it is customary to express $f_i(x)$ as a product of a density-independent term $F_i \geq 0$ and a density-dependent term $\hat{f}(x)$, i.e. $f_i(x) = F_i \hat{f}(x)$. Other possibilities are to express f_i as $f_i(y)$ where $y = \sum a_i x_i$, i.e. a weighted sum of age classes, or $f_i(x_i)$ which means that only age class i contributes to density effects. Frequently used fecundity functions may be found among members of the Deriso–Schnute family $f_i(x) = F_i(1 - \gamma \alpha x)^{1/\gamma}$. Observe that when $\gamma \to 0$ $f_i(x)$ equals the well-known overcompensatory Ricker relation $f_i(x) = F_i e^{-\alpha x}$, and when $\gamma = -1$, $f_i(x) = F_i(1 + \alpha x)^{-1}$ which is nothing but the compensatory Beverton and Holt formula. In cases where it is natural to consider density-dependent survival probabilities, we adopt the same strategy as above and write $p_i(x) = P_i \hat{p}(x)$ where $0 < P_i \leq 1$. Finally, from a biological point of view, we shall assume $f'(x) \leq 0$ and $p'(x) \leq 0$.

Map (1a) or (1b) may serve as excellent tools in order to reveal the dynamics of species with a wide range of different life histories. Species possessing precocious semelparous life histories, which is characterized by rapid development followed by only one reproduction, exemplified by annual plants, may be scrutinized by letting $n = 2$ and $F_1 = 0$. Species like cicadas and salmons possess delayed semelparous life histories. They live for many years and reproduce only once just before they die. 'Translated' to the Leslie matrix (2), this means that $F_1 = \cdots = F_{n-1} = 0$ and $F_n > 0$. Whenever all or most age classes are fertile, we say that the species exhibit a precocious

iteroparous life history. Examples may be found among small rodent populations, in particular when $n \leq 4$. In the final case, delayed iteroparity, we find species who live through several years before maturity and then survive to reproduce for many years. Humans and large mammals belong to this subclass. Regarding the Leslie matrix, this corresponds to $F_1 = \cdots = F_k = 0$, $F_{k+1} > 0, \ldots, F_n > 0$.

3 Some general properties

We start by considering the case where $f_i(x) = F_i(1 - \gamma \alpha x)^{1/\gamma}$, $i = 1, \ldots, n$ (which means that the fecundities belong to the Deriso–Schnute family) and constant year-to-year survival probabilities $p_i = P_i$, $i = 1, \ldots, n - 1, 0 < P_i \leq 1$, that is

$$x_{1,t+1} = \sum_{i=1}^{n} F_i(1 - \gamma \alpha x)^{1/\gamma} x_{i,t}$$
$$x_{2,t+1} = P_1 x_{1,t} \tag{3}$$
$$\vdots$$
$$x_{n,t+1} = P_{n-1} x_{n-1,t}$$

Let $L_i = P_1 P_2 \cdots P_{i-1}$, where $L_1 = 1$ and define the net inherent reproductive number as

$$R_0 = L_1 F_1 + \cdots + L_n F_n = \sum_{i=1}^{n} L_i F_i \tag{4}$$

and throughout the paper we will assume $R_0 > 1$ in order to obtain a feasible equilibrium population

$$x^* = \frac{1}{\gamma \alpha}\left(1 - R_0^{-\gamma}\right) \tag{5}$$

The equilibrium point of (3) may be expressed as

$$\begin{aligned}&\left(x_1^*, \ldots, x_i^*, \ldots, x_n^*\right)\\&= \left(\frac{L_1}{K}x^*, \ldots, \frac{L_i}{K}x^*, \ldots, \frac{L_n}{K}x^*\right)\end{aligned} \tag{6}$$

where $K = \sum_{i=1}^{n} L_i$.

Regarding stability properties of (6), we find under the assumption $F_1 = \cdots = F_n = F$ (which is a reasonable assumption for many species who possess a precocious iteroparous life history), that the eigenvalues λ of the linearization of (3) satisfy the equation

$$\lambda^n - \frac{1}{K} \sum_{i=1}^{n} L_i \left(\frac{1 - (\gamma + 1)\alpha x^*}{1 - \gamma \alpha x^*}\right) \lambda^{n-i} = 0 \tag{7}$$

Here, we may notice, due to (5), that α drops out of the equation. Therefore, we shall in the following assume $\alpha = 1$. The equilibrium point (6) is stable as long as all eigenvalues of (7) are located on the inside of the unit circle $|z| = 1$ in the complex plane.

Theorem 1 *Assume that $F_1 = \cdots = F_n = F$. Then, equilibrium point (6) of map (3) is always locally asymptotic stable provided*

$$x^* < \frac{2}{2\gamma + 1} \tag{8}$$

where x^* is given by (5).

Proof Let

$$P_n(\lambda) = \lambda^n - \frac{1}{K} \sum_{i=1}^{n} L_i \left(\frac{1 - (\gamma + 1)x^*}{1 - \gamma x^*} \right) \lambda^{n-i}$$

$$= 0$$

and assume that $|(1 - [\gamma + 1]x^*)(1 - \gamma x^*)^{-1}| < 1$. Then, write the left-hand side of the equation as $P_n(\lambda) = g(\lambda) + h(\lambda)$ where $g(\lambda) = \lambda^n$ and $h(\lambda)$ consist of the remaining terms. Clearly, g and h are analytic functions on and inside the unit circle $|z| = 1$ and the equation $g(\lambda) = 0$ has n roots inside $|z| = 1$. On the boundary, we have

$$\left| -\frac{1}{K} \sum L_i \left(\frac{1 - (\gamma + 1)x^*}{1 - \gamma x^*} \right) \right|$$

$$\leq \left| \frac{L_1}{K} \left(\frac{1 - (\gamma + 1)x^*}{1 - \gamma x^*} \right) \right|$$

$$+ \cdots + \left| \frac{L_n}{K} \left(\frac{1 - (\gamma + 1)x^*}{1 - \gamma x^*} \right) \right|$$

$$\leq \left| \frac{1 - (\gamma + 1)x^*}{1 - \gamma x^*} \right| < |g(\lambda)| = 1$$

Then, according to Rouché's theorem $P_n(\lambda) = g(\lambda) + h(\lambda)$ and $g(\lambda)$ have the same number of zeros located inside the unit circle, i.e. n-zeros, which proves that $|(1 - [\gamma + 1]x^*)(1 - \gamma x^*)^{-1}| < 1$ is sufficient to guarantee a stable equilibrium which is equivalent to say

$$x^* < \frac{2}{2\gamma + 1}$$

$\square$

Hence, in the Ricker case ('worst' case), $x^* < 2$, $\gamma = -1/4$ implies $x^* < 4$, $\gamma = -1/3$ implies $x^* < 6$ and in the Beverton and Holt case the equilibrium point will

always be stable. Note that the regions above ($x^* < a$) are regions where stability is guaranteed. Depending on the number of age classes and parameters, the actual instability thresholds may be larger.

4 2-Age classes

When $n = 2$, $\alpha = 1$ and $F_1 = F_2 = F$, equilibrium point (6) may be expressed as

$$(x_1^*, x_2^*) = \left(\frac{1}{1 + P_1}x^*, \frac{P_1}{1 + P_1}x^* \right) \tag{9}$$

where $R_0 = F(1 + P_1)$ and x^* is given by (5). The corresponding eigenvalue Eq. (7) is on the form

$$\lambda^2 + a_1\lambda + a_2 = 0 \tag{10}$$

where

$$a_1 = (f'x^* + f) = -\frac{1}{1 + P_1} \left(1 - \frac{x^*}{1 - \gamma x^*} \right)$$

$$a_2 = P_1(f'x^* + f) = -\frac{P_1}{1 + P_1} \left(1 - \frac{x^*}{1 - \gamma x^*} \right)$$

and f, f' are evaluated at equilibrium. In order for (x_1^*, x_2^*) to be locally asymptotic stable, the Jury criteria

$$1 + a_1 + a_2 > 0 \tag{11a}$$

$$1 - a_1 + a_2 > 0 \tag{11b}$$

$$1 - |a_2| > 0 \tag{11c}$$

must hold. Easy calculations show that (11a) is satisfied for any $x^* > 0$. Hence, (x_1^*, x_2^*) will never experience a saddle node bifurcation at instability threshold. (11b) may be written as $(1 + 2\gamma - P_1)x^* < 2$. If $\gamma \leq (P_1 - 1)/2$, then (11b) is valid for any $x^* > 0$. Whenever $\gamma > (P_1 - 1)/2$, (11b) holds if $x^* < 2/(1 + 2\gamma - P_1)$ and a flip bifurcation will occur at threshold $x^* = 2/(1 + 2\gamma - P_1)$ for x^* sufficiently large. Regarding (11c), $(P_1 + [1 + 2P_1]\gamma)x^* < 1 + 2P_1$, it holds for any $x^* > 0$ provided $\gamma \leq -P_1/(1 + 2P_1)$. When $\gamma > -P_1/(1 + 2P_1)$, (11c) is still valid if $x^* < (1 + 2P_1)/(P_1 + [1 + 2P_1]\gamma)$ and (x_1^*, x_2^*) will lose its hyperbolicity through a Neimark–Sacker (hereafter shortened NS) bifurcation at threshold $x^* = (1 + 2P_1)/(P_1 + [1 + 2P_1]\gamma)$.

Thus, if $\gamma \leq (P_1 - 1)/2$ and $\gamma \leq -P_1/(1 + 2P_1)$, then (x_1^*, x_2^*) will be locally asymptotic stable for any $x^* > 0$. Whenever $\gamma > (P_1 - 1)/2$,
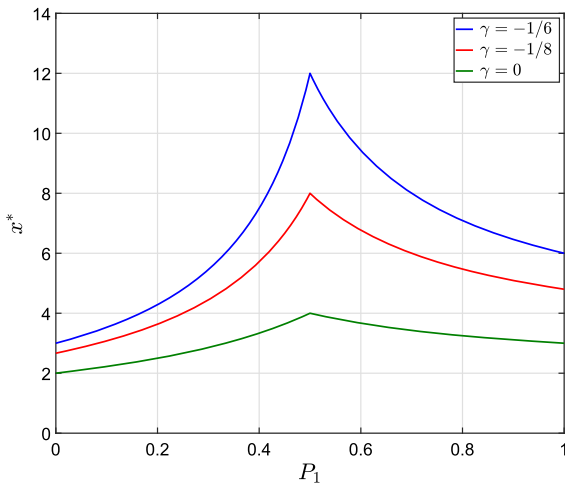
Fig. 1 Graphs that separate stable and unstable parameter regions in the case $\gamma = -1/6$ (blue graph), $\gamma = -1/8$ (red graph) and $\gamma \to 0$ (green graph). The stable parameter regions are located below the graphs

$\gamma > -P_1/(1 + 2P_1)$ and $x^* < \min\{2/(1 + 2\gamma - P_1), (1+2P_1)/(P_1+\gamma[1+2P_1])\}$, the equilibrium will also be stable. At thresholds $x^* = 2/(1 + 2\gamma - P_1)$, $x^* = (1 + 2P_1)/(P_1 + \gamma[1 + 2P_1])$, (x_1^*, x_2^*) will undergo a flip or a NS bifurcation respectively. If a flip shall occur prior to a NS bifurcation, then

$$\frac{2(P_1 - 1/2)(P_1 + 1)}{(1 + 2\gamma - P_1)(P_1 + \gamma(1 + 2P_1))} < 0 \tag{12}$$

In Fig. 1, we show the graphs that separate stable and unstable parameter regions in the cases $\gamma = -1/6$, $\gamma = -1/8$ and $\gamma \to 0$ and clearly, the larger the γ, the smaller the stable parameter region.

Our next goal is to scrutinize what happens at the various instability thresholds and we start by considering the interval $0 < P_1 < 1/2$.

Theorem 2 *Consider the map*

$$(x_1, x_2) \mapsto (F(1 - \gamma x)^{1/\gamma} x_1 \\ + F(1 - \gamma x)^{1/\gamma} x_2, P_1 x_1) \tag{13}$$

whose equilibrium is

$$(x_1^*, x_2^*) = \left(\frac{1}{1 + P_1} x^*, \frac{P_1}{1 + P_1} x^*\right)$$

where

$$x^* = \frac{1}{\gamma}\left(1 - (F(1 + P_1))^{-\gamma}\right)$$

Then, in case of $\gamma > (P_1 - 1)/2$ and a fixed P_1, $0 < P_1 < 1/2$, (x_1^*, x_2^*) will undergo a supercritical flip bifurcation at threshold

$$x^* = \frac{2}{1 + 2\gamma - P_1}$$

$$\Leftrightarrow F = \frac{1}{1 + P_1}\left(\frac{1 + 2\gamma - P_1}{1 - P_1}\right)^{1/\gamma} \tag{14}$$

Hence, when (x_1^*, x_2^*) fails to be stable, an attracting period 2 orbit is established. For a formal proof, confer Appendix A.

Regarding the dynamics beyond instability threshold the results are as follows: As proved, independent of the value of P_1 ($0 < P_1 < 1/2$) there will always be an F interval just beyond threshold (14) where we find stable orbits of period 2. Through further increase of F there may be stable orbits of period 2^k as well as chaotic dynamics as exemplified in the bifurcation diagram, Fig. 2a blue graph, and the Lyapunov exponent graph, Fig. 2b blue graph, in the case $\gamma \to 0$ (i.e. $F(1 - \gamma x)^{1/\gamma} = Fe^{-x}$) and $P_1 = 0.4$. (If the Lyapunov exponent $L < 0$, it corresponds to a stable fixed point or a stable periodic orbit, $L = 0$ means that the dynamics occurs on an attracting invariant curve, while $L > 0$ corresponds to chaotic oscillations). However, in nonlinear systems one may not rule out the possibility of multiple attractors. Indeed, still referring to Fig. 2a, in the interval $34.18 < F < 39.42$ we observe that the stable 2-cycle coexists with a 3-cycle red graph and in case of larger values of F there is coexistence between the 2-cycle and a chaotic attractor which disappears when $F = 46.13$. The structure of the attractor is displayed in Fig. 3a and b; we provide a corresponding time-series graph. Coexistence has also been detected for smaller values of γ. For example, when $\gamma = -1/6$ the 3-cycle coexists with (x_1^*, x_2^*) as well, and the smaller the γ, the larger becomes the F interval where coexistence is possible. Hence, in all intervals where we find coexistence, the ultimate fate of an orbit depends on the initial condition. We postpone a more thorough analysis of the 3-cycle to the $P_1 = 1$ case.

When $P_1 = 1/2$, the solution of the eigenvalue Eq. (10) at instability threshold becomes $\lambda_1 = \lambda_2 = -1$, i.e. a codimension 2 bifurcation which is also referred to as a 1 : 2 resonance, cf [30] (p. 411). In this case, the procedure used in order to prove Theorem 2 does not apply anymore. Instead we have the following result:
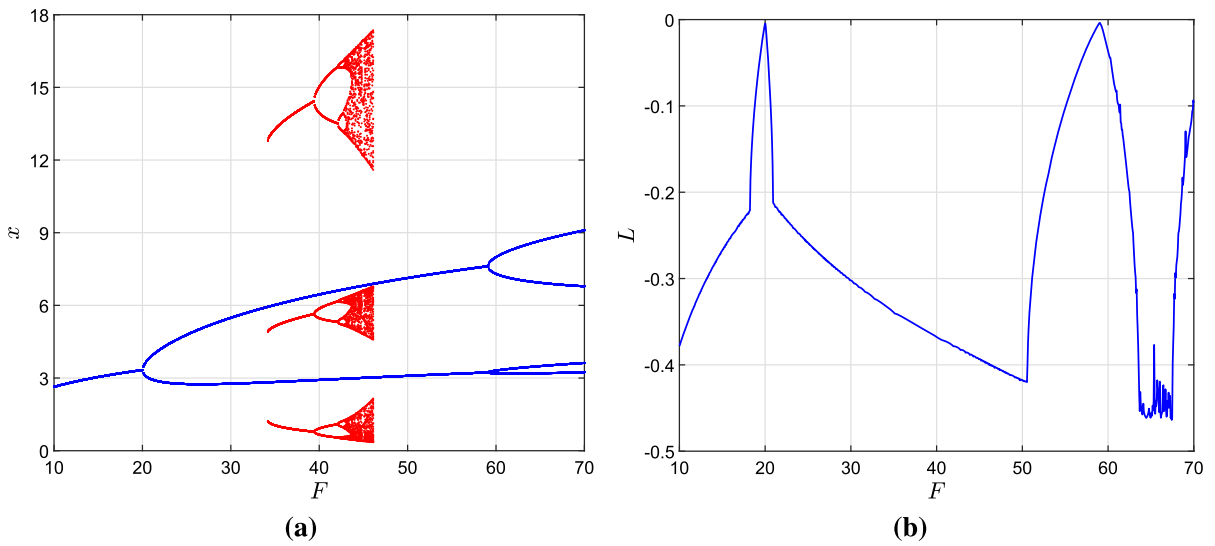
(a)   **(b)**

Fig. 2 **a** Bifurcation diagram generated by map (13). $\gamma = 0$, $P_1 = 0.4$. **b** Values of Lyapunov exponent L

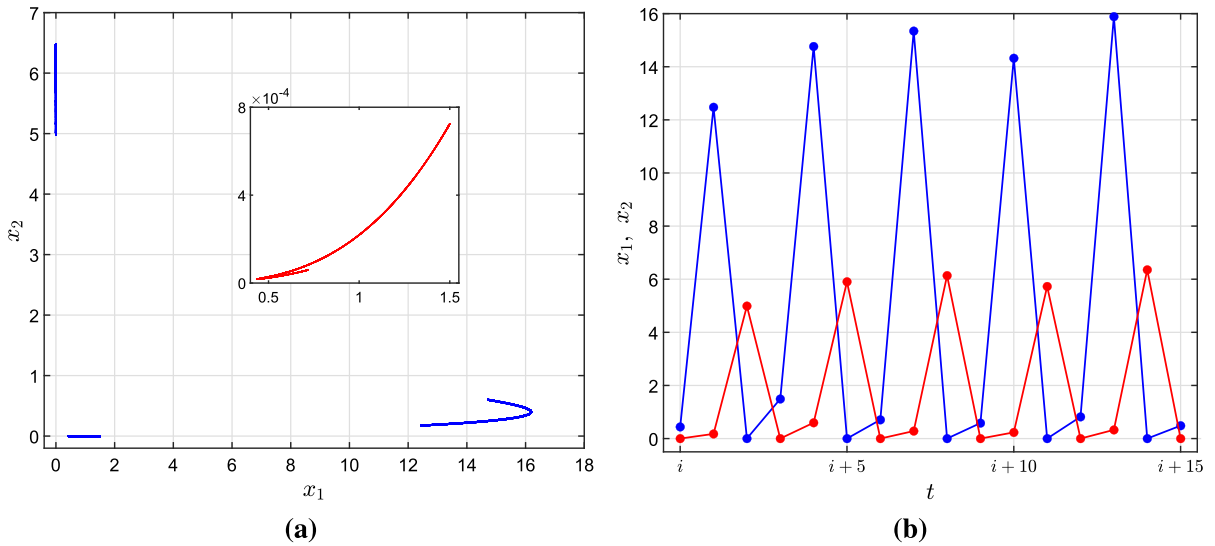**(a)**   **(b)**

Fig. 3 **a** Chaotic attractor (blue graph) generated by map (13) when $(P_1, F) = (0.4, 44)$ together with a magnification of the lower left branch (red graph). Initial values $(x_{1,0}, x_{2,0}) =$

$(0.5, 6.0)$. **b** Time series obtained from map (13), x_1 blue and x_2 red. Same parameters as in **a**

Theorem 3 *Assume $P_1 = 1/2$ and $-1/4 < \gamma < 0$. Then map (13) undergoes a $1 : 2$ resonance at threshold $x^* = 4/(1 + 4\gamma)$ and the map may be cast in $1 : 2$ resonance form as*

$$\begin{pmatrix} \xi_1 \\ \xi_2 \end{pmatrix} \mapsto \begin{pmatrix} -1 & 1 \\ \beta_1 & -1 + \beta_2 \end{pmatrix} \begin{pmatrix} \xi_1 \\ \xi_2 \end{pmatrix}$$

$$+ \begin{pmatrix} 0 \\ C(\overline{\beta})\xi_1^3 + D(\overline{\xi})\xi_1^2\xi_2 \end{pmatrix} \quad (15)$$

where

$$C(0) = \frac{1}{18}(4\gamma + 1)^2(-4\gamma^2 + 3\gamma - 2)$$

$$D(0) = \frac{1}{9}(4\gamma + 1)^2(8\gamma^2 - 5\gamma + 5)$$

For a formal proof confer Appendix B.

Now, in order to analyse in somewhat more detail what happens at threshold, one possibility is to approximate (15) by a flow. However, since the eigenvalues of the matrix are negative when $\overline{\beta} = 0$, this will not work. Therefore, we consider the second iterate of (15) which in difference equation form may be expressed as

$$\begin{pmatrix} \xi_1 \\ \xi_2 \end{pmatrix}_{t+2} = \begin{pmatrix} 1 + \beta_1 & -2 + \beta_2 \\ -2\beta_1 + \beta_1\beta_2 & 1 + \beta_1 - 2\beta_2 + \beta_2^2 \end{pmatrix} \\ \begin{pmatrix} \xi_1 \\ \xi_2 \end{pmatrix}_t + \begin{pmatrix} E(\overline{\xi}_t, \overline{\beta}) \\ F(\overline{\xi}_t, \overline{\beta}) \end{pmatrix} \quad (16)$$

where

$$E(\overline{\xi}, \overline{\beta}) = C(\overline{\beta})\xi_1^3 + D(\overline{\beta})\xi_1^2\xi_2$$

and

$$\begin{aligned} F(\overline{\xi}, \overline{\beta}) &= \Big(-2C(\overline{\beta}) + \beta_1 D(\overline{\beta}) + \beta_2 C(\overline{\beta}) \Big)\xi_1^3 \\ &+ \Big(3C(\overline{\beta}) - 2D(\overline{\beta}) - 2\beta_1 D(\overline{\beta}) \\ &+ \beta_2 D(\overline{\beta}) \Big)\xi_1^2\xi_2 + \Big(-3C(\overline{\beta}) + 2D(\overline{\beta}) \\ &+ \beta_1 D(\overline{\beta}) - 2\beta_2 D(\overline{\beta}) \Big)\xi_1\xi_2^2 \\ &+ \Big(C(\overline{\beta}) - D(\overline{\beta}) + \beta_2 D(\overline{\beta}) \Big)\xi_2^3 + O(|\xi|^4) \end{aligned}$$

and any nontrivial fixed point of (16) corresponds to a single period to orbit of (15). Moreover, following the procedure outlined in [30] it is possible to approximate (16) by a flow which may be cast in the form

$$\begin{pmatrix} \dot{\eta}_1 \\ \dot{\eta}_2 \end{pmatrix} = \begin{pmatrix} 0 & 1 \\ \epsilon_1 & \epsilon_2 \end{pmatrix}\begin{pmatrix} \eta_1 \\ \eta_2 \end{pmatrix} \\ + \begin{pmatrix} 0 \\ C_1\eta_1^3 + D_1\eta_1^2\eta_2 \end{pmatrix} + O(|\eta|^4) \quad (17)$$

where

$$\begin{aligned} \epsilon_1 &= \epsilon_1(\overline{\beta}) = 4\beta_1 + O(|\beta|^2) \\ \epsilon_2 &= \epsilon_2(\overline{\beta}) = -2\beta_1 - 2\beta_2 \\ C_1 &= C_1(\overline{\beta}) \\ D_1 &= D_1(\overline{\beta}) \end{aligned}$$

such that

$$\begin{aligned} C_1(0) &= 4C(0) = \frac{2}{9}(4\gamma + 1)^2\big(-4\gamma^2 + 3\gamma - 2 \big) \\ &< 0 \\ D_1(0) &= -2D(0) - 6C(0) \end{aligned}$$

$$= -\frac{1}{9}(4\gamma + 1)^2\big(4\gamma^2 - \gamma + 4\big) < 0$$

so the nondegeneracy conditions $C_1(0) \neq 0$, $D_1(0) \neq 0$ hold. Finally, by use of $s = \text{sign } C_1(0) = -1$, $D_1(0) < 0$ and scaling we may rewrite (17) as

$$\begin{aligned} \dot{\Omega}_1 &= \Omega_2 \\ \dot{\Omega}_2 &= \delta_1\Omega_1 + \delta_2\Omega_2 + s\Omega_1^3 - \Omega_1^2\Omega_2 \end{aligned} \quad (18)$$

Clearly, $(0, 0)$ is a trivial fixed point of (18) and since $s = -1$ there are also two nontrivial fixed points of the form $(\pm\sqrt{\delta_1}, 0)$ provided $\delta_1 > 0$. Moreover, $(0, 0)$ bifurcates to $(\pm\sqrt{\delta_1}, 0)$ through a pitchfork bifurcation at $\delta_1 = 0$. Now, if we relate our findings above to our original discrete system (16) the nontrivial fixed point corresponds to a period 2 orbit of (15). Consequently, when $P_1 = 1/2$ the fixed point will bifurcate to a stable period 2 orbit.

Next, focus on the P_1 interval $1/2 < P_1 < 1$.

Theorem 4 *If $1/2 < P_1 < 1$ and $-P_1/(1 + 2P_1) < \gamma < 0$ the fixed point (x_1^*, x_2^*) of map (13) will undergo a supercritical NS bifurcation at threshold*

$$\begin{aligned} x^* &= \frac{1 + 2P_1}{P_1 + \gamma(1 + 2P_1)} \\ &\Leftrightarrow F = \frac{1}{1 + P_1}\left(1 + \gamma\frac{1 + 2P_1}{P_1}\right)^{1/\gamma} \end{aligned} \quad (19)$$

For a formal proof see Appendix C.

From Theorem 4, it follows that when (x_1^*, x_2^*) fails to be stable, an attracting invariant curve is established and in Fig. 4 we show such a curve in the case $\gamma \to 0$ (Ricker Case) and $(P_1, F) = (0.6, 26)$. On such a curve map (13) is topologically equivalent to a circle map with associated irrational rotation number σ. However, as a result of increasing the fecundity, σ approaches $1/5$ and through frequency locking there exists an F interval where the invariant curve turns to a 5-cyclic attractor. This scenario is displayed in the bifurcation diagram in Fig. 5a, as well as in the Lyapunov exponent diagram, Fig. 5b. For larger values of P_1, the dynamics may change. Indeed, cf Fig. 6a, when $P_1 = 0.8$ there exist parameter intervals $F_3 \leq F \leq F_B$ and $F_B \leq F \leq F_C$ where the stable fixed point (first interval) and an invariant curve (second interval) coexist with a stable 3-cycle with large amplitude, respectively. The 3-cycle is created at $F_3 = 11.851$ (through a saddle node bifurcation) and

disappears when $F = F_C = 16.216$. $F_B = 14.328$ is the bifurcation value computed from (19). Regarding the trapping regions we have the following: When $F > F_3$ but $F - F_3$ is small the trapping region for the invariant curve consist of all initial points located on the inside of the curve as well as three regions outside the curve as displayed in Fig. 6c. Through an increase of F but $F < F_C$ the regions of points outside the invariant curve become smaller and when F is located close to F_C the trapping region for the invariant curve consists mostly of points located on the inside of the curve, as illustrated in Fig. 6d. The rationale behind this may be understood along the following line. Through the saddle node bifurcation at $F = F_3$, three branches of unstable (repelling) points are created too. When $F > F_B$ but $F - F_B$ is small the distance between these branches and the invariant curve is 'large', hence the invariant curve is perfectly capable of attracting points located at some distance outside the curve. However, as F is approaching F_C the branches of unstable points are located very close to the invariant curve. Hence, a majority of points in the vicinity (outside) the invariant curve are pushed away from the region and towards the stable 3-cycle. Consequently, the trapping region for the invariant curve consists mainly of points located on the inside of the curve. Whenever $F > F_C$ but $F - F_C$ is small the 3-cycle is the only attractor and as F is further increased periodic orbits of period $3 \cdot 2^k$ are established and eventually the dynamics becomes chaotic. These findings are visualized in Fig. 6a and b. Thus an increase of P_1 acts in a destabilizing fashion. When $P_1 \to 1$, the value of λ approaches third root of unity which implies that $\sigma \to 1/3$. Thus, in this part of parameter space the large 3-cycle coexists with an almost 3-periodic orbit restricted to an invariant curve as accounted for in Fig. 7. The ultimate fate on an orbit depends on the initial condition. The trapping region for the invariant curve consists almost exclusively of initial points located on the inside of the curve.

Next, consider smaller values of γ, and as proved, smaller values of γ imply better stability properties. For example, when $P_1 = 0.8$ we find from Theorem 4 in the Ricker case ($\gamma \to 0$) that (x_1^*, x_2^*) undergoes a supercritical NS bifurcation when $F = 14.33$ while the corresponding bifurcations when $\gamma = -1/8$ and $\gamma = -1/6$ occur at $F = 35.97$ and $F = 59.93$ respectively. Otherwise the qualitative picture is in many respects quite similar. However, since (x_1^*, x_2^*) is stable in much larger F intervals we find that the fixed point when
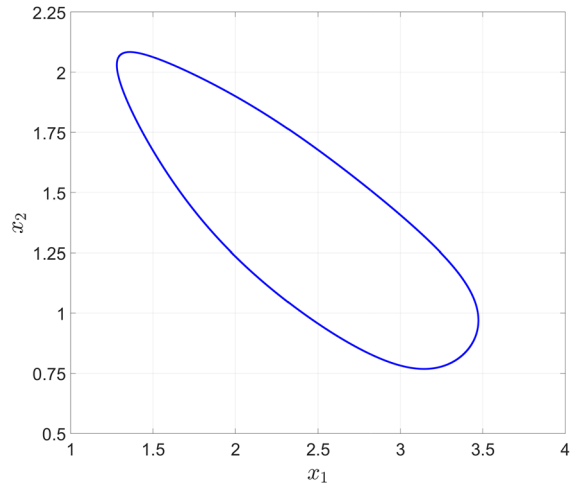

Fig. 4 An invariant curve generated by map (13), $\gamma \to 0$ and $(P_1, F) = (0.6, 26)$

$P_1 = 0.8$ may coexist with $3 \cdot 2^k$ cycles which we do not find when $\gamma \to 0$. Actually, when $P_1 = 0.6$ there exists an interval where (x_1^*, x_2^*) coexists with a chaotic attractor.

Next, consider the remaining case $P_1 = 1$. At instability threshold λ equals third root of unity ($\lambda = -1/2 \pm 1/2 \cdot \sqrt{3}i$), and in accordance with [30], we refer to this case as the 1:3 resonance case. $P_1 = 1$ implies that the normal form of map (13) (cf Eq. (C.8) in Appendix C) contains an additional resonant term of degree 2 and we have the following result:

Theorem 5 *If $P_1 = 1$ and $-1/3 < \gamma < 0$ map (13) undergoes a $1 : 3$ resonance and may be written in complex form as*

$$w_{t+1} = \lambda w_t + C(\gamma)\overline{w}_t^2 + D(\gamma)w_t|w_t|^2 \\ + O\left(|w_t|^4\right) \qquad (20)$$

where

$$C(\gamma) = -\frac{1 - 9\gamma^2}{16\sqrt{3}}\left(\sqrt{3} - i\right)$$

$$D(\gamma) = \frac{(1 + 3\gamma)^2}{192}\left(9\gamma^2 + 6\gamma + 5 + \sqrt{3}\gamma(3\gamma - 7)i\right)$$

For a formal proof, confer Appendix D.

Next, consider the dynamics. As accounted for there are F intervals both when $P_1 < 1/2$ and $P_1 > 1/2$ where a stable 3-cycle coexists with the stable fixed point (x_1^*, x_2^*). Moreover, when $P_1 > 1/2$, the 3-cycle may
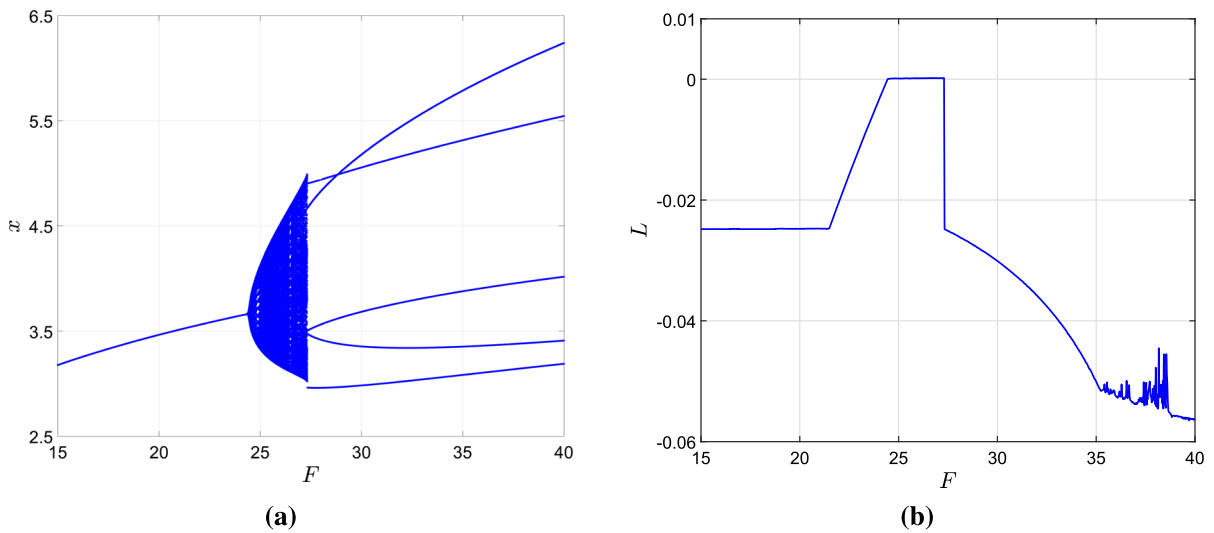
Fig. 5 **a** Bifurcation diagram generated by map (13) when $\gamma \to 0$ and $P_1 = 0.6$. **b** Values of Lyapunov exponent L when $P_1 = 0.6$

coexist with an invariant curve as well but the F intervals where this occurs shrink as P_1 approaches unity. Now, considering the 3-cycle, we have verified numerically that it is established as the third iterate of map (13) undergoes a saddle node bifurcation. When $P_1 = 1$, this occurs in the Ricker case when $F = F_K = 8.9438$. Hence, at $F = F_K$ three branches of stable equilibria are born but also three branches of unstable equilibria. In Fig. 8, we see two stable branches (solid lines). (The reason that we see two and not three is that when $P_1 = 1$ the sum $x = x_1 + x_2$ is the same for two of the points in the cycle. For example, when $F = 10.5$ the points in the cycle are $(3.8300, 0.5680)$, $(0.5680, 3.8300)$ and $(0.5680, 0, 5680)$, but the sum $x = x_1 + x_2$ is the same for the first two points). The figure also displays the branches of unstable points (dashed lines). It is a tedious task to compute these points, but we have managed to do so by backward iterations

$$\begin{pmatrix} x_{1,t} \\ x_{2,t} \end{pmatrix} = \begin{pmatrix} 0 & 1 \\ (Fe^{-x_t})^{-1} & -1 \end{pmatrix} \begin{pmatrix} 0 & 1 \\ (Fe^{-x_{t+1}})^{-1} & -1 \end{pmatrix}$$

$$\begin{pmatrix} 0 & 1 \\ (Fe^{-x_{t+2}})^{-1} & -1 \end{pmatrix} \begin{pmatrix} x_{1,t+3} \\ x_{2,t+3} \end{pmatrix} \quad (21)$$

where x_{t+2}, x_{t+1} and x_t satisfy

$$x_{t+2} = W_0 \left(\frac{x_{1,t+3}}{F} \right)$$

$$x_{t+1} = W_0 \left(\frac{x_{2,t+2}}{F} \right)$$

$$x_t = W_0 \left(\frac{x_{t+2} - x_{2,t+3}}{F} \right)$$

and W_0 is the Lambert function. Therefore, from our calculations and Fig. 8, we conclude that (x_1^*, x_2^*) undergoes a subcritical bifurcation at $(P_1, F) = (1, (1/2)e^3)$ where it collides with the three branches of unstable periodic points generated by the third iterate of (13). Consequently, when F exceeds threshold $(1/2)e^3$ and $|F - (1/2)e^3|$ is small the only attractor is the 3-cycle which in turn bifurcates to orbits of period $3 \cdot 2^k$ and chaotic dynamics through further enlargement of F. Finally, our conjecture is that a similar phenomenon occurs for smaller values of P_1 as well. Referring to Fig. 6a, the invariant curve disappears when $F = 16.125$. Numerical experiments clearly suggest that this happens as the curve is hit by branches of unstable periodic points generated by the third iterate of (13) at $F = 11.851$.

5 3-Age classes

Next, let us focus on three age classes, i.e. the map

$$(x_1, x_2, x_3) \mapsto \big(F_1 (1 - \gamma \alpha x)^{1/\gamma} x_1 + F_2 (1 - \gamma \alpha x)^{1/\gamma} x_2$$
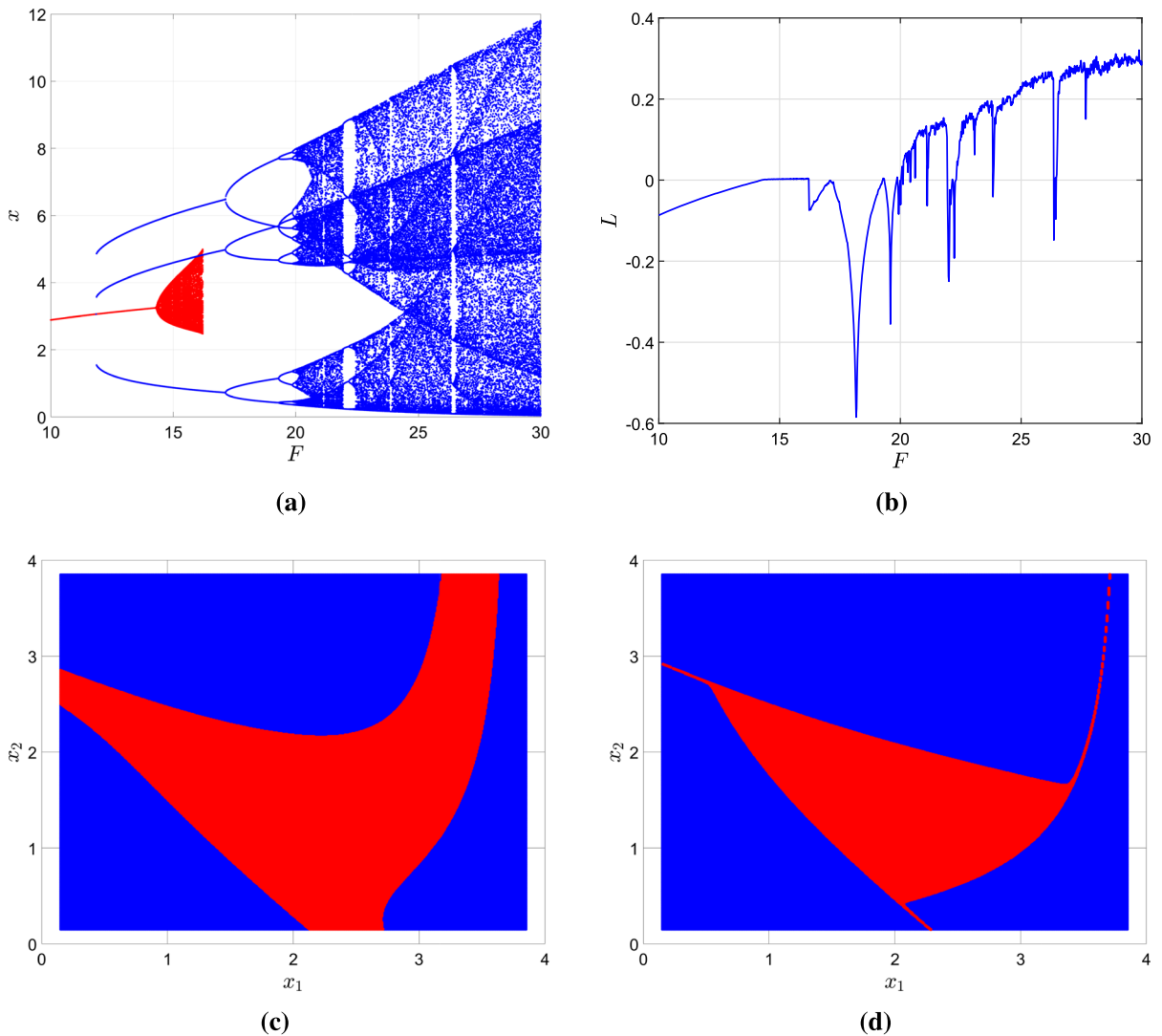$$+ F_3 (1 - \gamma \alpha x)^{1/\gamma} x_3, P_1 x_1, P_2 x_2 \big) \quad (22)$$

Fig. 6 **a** Bifurcation diagram generated by map (13) when $\gamma \to 0$ and $P_1 = 0.8$. **b** Values of Lyapunov exponent L when $P_1 = 0.8$. **c** Trapping region (red) for the invariant curve, $F = 14.5$. **d** Trapping region (red) for the invariant curve, $F = 16.215$

By use of results from Sect. 3 we find the nontrivial fixed point as

$$(x_1^*, x_2^*, x_3^*) = \left(\frac{1}{1 + P_1 + P_2} x^*, \frac{P_1}{1 + P_1 + P_2} x^*, \right.$$
$$\left. \frac{P_1 P_2}{1 + P_1 + P_2} x^* \right) \qquad (23)$$

where

$$x^* = \frac{1}{\gamma \alpha} \left(1 - R_0^{-\gamma} \right)$$

$$R_0 = \sum_{i=1}^{3} L_i F_i$$

Moreover, assuming $\alpha = 1$ and equal fecundities ($F_1 = F_2 = F_3 = F$) the eigenvalue equation may be cast in the form

$$\lambda^3 + a_1 \lambda^2 + a_2 \lambda + a_3 = 0 \qquad (24)$$

where

$$a_1 = -\frac{1}{1 + P_1 + P_1 P_2} \left(\frac{1 - (\gamma + 1)x^*}{1 - \gamma x^*} \right)$$
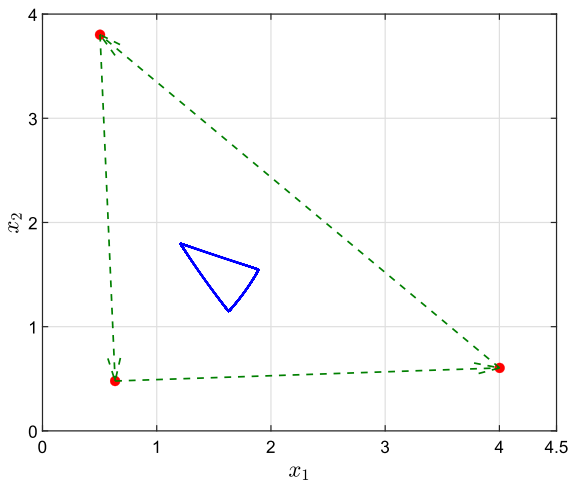
Fig. 7 Coexisting attractors. $(P_1, F) = (0.95, 10.945)$, with initial conditions $(x_{1,0}, x_{2,0}) = (0.7, 3.3)$ and $(x_{1,0}, x_{2,0}) = (1.6, 1.4)$ for the 3-cycle and almost 3 periodic orbit, respectively

Fig. 8 Branches of stable points (solid lines) and unstable points (dashed lines) generated by the third iterate of map (13) together with (x_1^*, x_2^*) generated by map (13), $P_1 = 1$ (Ricker case)

$$a_2 = P_1 a_1$$

$$a_3 = P_1 P_2 a_1$$

In order for the fixed point to be stable, the eigenvalues λ must satisfy $|\lambda| < 1$ which is ensured whenever the Jury criteria

$$1 + a_1 + a_2 + a_3 > 0 \tag{25a}$$

$$1 - a_1 + a_2 - a_3 > 0 \tag{25b}$$

$$1 - |a_3| > 0 \tag{25c}$$

$$|1 - a_3^2| - |a_2 - a_3 a_1| > 0 \tag{25d}$$

are satisfied. Now, in case of $x^* \approx (\gamma + 1)^{-1}$ all coefficients a_i are close to zero and subsequently all four criteria clearly hold. Hence, fixed point (23) (equal fecundities) is locally asymptotic stable in case of x^* small. Criteria (25a) hold for any $x^* > 0$. Denoting the values of x^* where (25b)–(25d) fail for x_F^*, x_{NS1}^* and x_{NS2}^*, respectively, we find after some algebra

$$x_F^* - x_{NS1}^*$$

$$= \frac{P_1^2 - 1 - P_1 P_2 (1 - P_1)}{\left(1 - P_1 + P_1 P_2 + 2\gamma(1 + P_1 P_2)\right)\left((1 + P_1 + 2P_1 P_2)\gamma + P_1 P_2\right)} < 0$$

Moreover, in order for $x_{NS2}^* - x_F^*$ to be negative, the inequality

$$(1 - P_1)(1 - 2P_1 + 3P_1 P_2) < 0 \tag{26}$$

must be satisfied. Therefore, whenever (26) is valid, a NS bifurcation will take place prior to a flip bifurcation
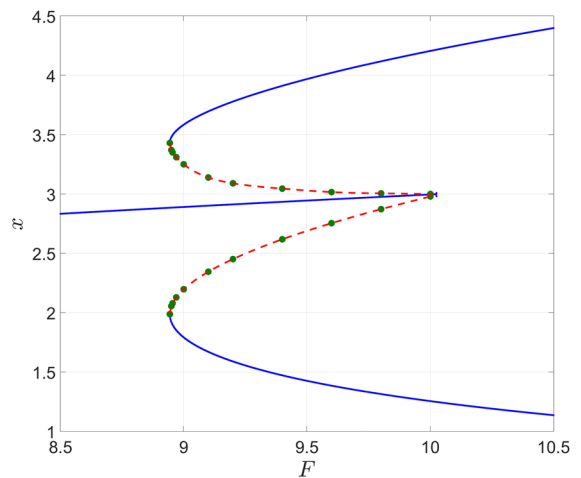
and this is only possible in parameter regions where $P_1 > \frac{1}{2}$ and $P_2 \ll P_1$. Thus, we conclude that in case of x^* small the fixed point (x_1^*, x_2^*, x_3^*) is stable and when x^* is increased (as a result of increasing F) a NS bifurcation will occur at threshold $x^* = x_{NS2}^*$ if $1 - 2P_1 + 3P_1 P_2 < 0$ or alternatively a flip bifurcation at threshold $x^* = x_F^*$ if $1 - 2P_1 + 3P_1 P_2 > 0$.

In Fig. 9a where $\gamma \to 0$ we have drawn the graphs of x_F^* and x_{NS2}^* in the cases $P_1 = 0.8$ (blue graph), $P_1 = 0.5$ (red graph) and $P_1 = 0.2$ (green graph). The stable parameter region is located below the graphs. When $P_1 = 0.2$ or 0.5 the transfer from stability to instability will always go through a flip bifurcation, but when $P_1 = 0.8$ and $P_2 < 0.25$, the fixed point will experience a NS bifurcation at threshold. Figure 9b, where $\gamma = -\frac{1}{10}$, displays qualitatively the same situation. The difference is that the size of x^* at threshold is larger which in many respects is nothing but a consequence of Theorem 1.

Next, assuming $x_F^* < x_{NS2}^*$, let us study the flip bifurcation in somewhat more detail. At threshold $x^* = x_F^*$, the value of F becomes

$$F = \frac{1}{1 + P_1 + P_1 P_2}\left(1 + \gamma \frac{2(1 + P_1 P_2)}{1 - P_1 + P_1 P_2}\right)^{1/\gamma} \tag{27}$$
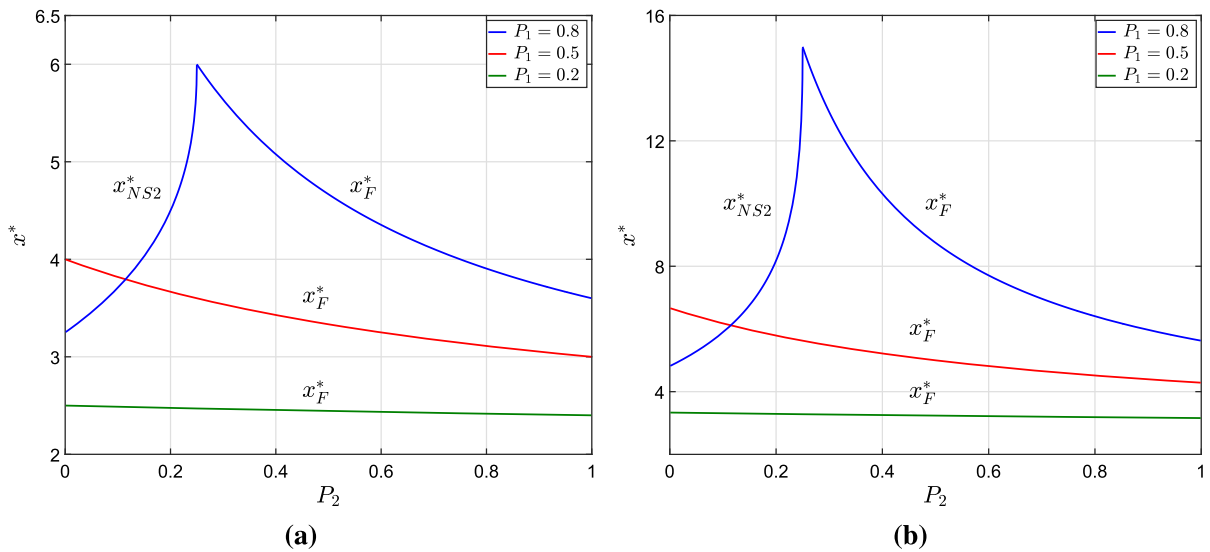
Fig. 9 Values of x_F^* and x_{NS2}^* in the cases $P_1 = 0.8$ (blue graph), $P_1 = 0.5$ (red graph) and $P_1 = 0.2$ (green graph). **a** $\gamma = 0$. **b** $\gamma = -1/10$

and from (24) we obtain the solutions

$$\lambda_1 = -1$$

$$\lambda_{2,3} = -\frac{P_1(1 - P_2)}{2(1 - P_1 + P_1 P_2)}$$

$$\pm \frac{\sqrt{4(1 - P_1 + P_1 P_2)P_1 P_2 - P_1^2(1 - P_2)^2}}{2(1 - P_1 + P_1 P_2)} i \tag{28}$$

with property

$$|\lambda_{2,3}| = \sqrt{\frac{P_1 P_2}{1 - P_1 + P_1 P_2}} < 1$$

Regarding the nature of the flip bifurcation we have the following result:

Theorem 6 *Assume* $0 < P_1 < 1$, $0 < P_2 < 1$ *and* $x_F^* < x_{NS2}^*$ *(i.e.* $1 - 2P_1 + 3P_1 P_2 > 0$*). Then, the fixed point* (23) *of map* (22) *where* $F_1 = F_2 = F_3 = F$ *will undergo a supercritical flip bifurcation at threshold* $x^* = x_F^*$.

For a formal proof, confer Appendix E.

Let us now turn to the dynamics. Assuming $x_F^* < x_{NS2}^*$, (which is the case in most of the parameter space), $\gamma = 0$, and $x^* > x_F^*$ Theorem 6 implies that as long as $|x^* - x_F^*|$ is small the dynamics is stable period 2 orbits. As we continue to increase x^* (as a result of

increasing F), stable orbits of period 4 are detected but through further enlargement of F a NS bifurcation occurs so the dynamics now turns quasiperiodic and is restricted to four disjoint invariant curves which are visited once every fourth iteration. This is exemplified in Fig. 10a. In case of larger values of F, the dynamics turns chaotic, confer the Lyapunov exponent calculations presented in Fig. 10b. For small negative values of γ, we find much of the same dynamics. The main difference is that the value of F and x^* at bifurcation threshold x_F^* is much larger which clearly suggests that a decrease of γ acts stabilizing. Otherwise, no other qualitative changes have been found.

Next, assuming $\gamma = 0$, consider $x_{NS2}^* < x_F^*$ and $x^* < x_{NS2}^*$ which occurs in regions where P_1 is 'large' and P_2 'small'. Here, through an increase of F, Jury criterion (25d) fails before criterion (25b) and subsequently the eigenvalues at bifurcation threshold are complex. Thus, at threshold $x^* = x_{NS2}^*$, the fixed point (x_1^*, x_2^*, x_3^*) undergoes a (supercritical) NS bifurcation. Hence, beyond threshold the dynamics is quasiperiodic. Through further enlargement of F the dynamics alternates between quasiperiodic orbits and periodic orbits of long period before it turns chaotic. Moreover, no qualitative changes have been observed for small negative values of γ.
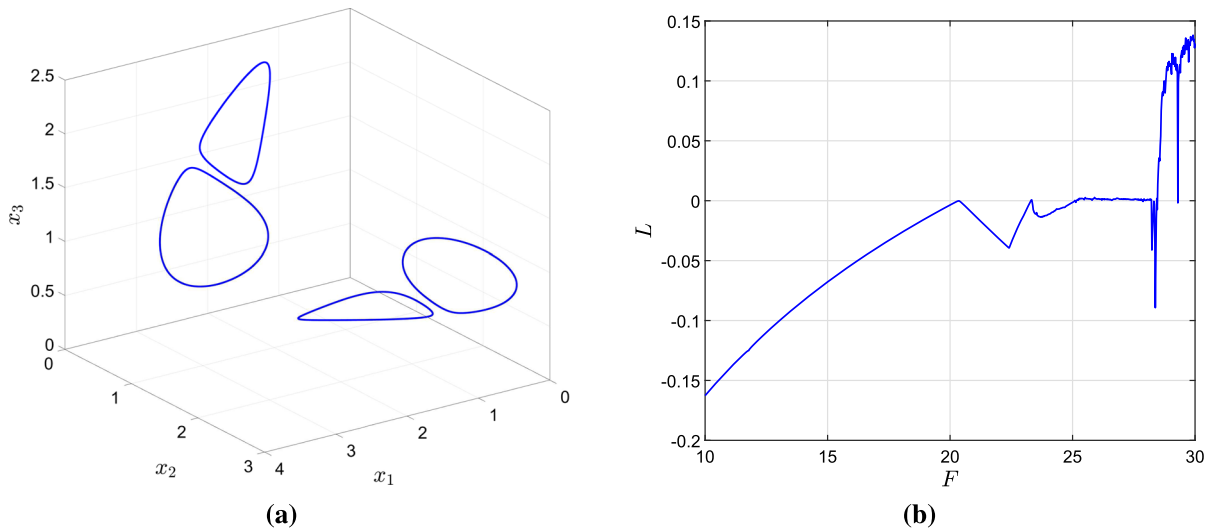
(a)

(b)

Fig. 10 **a** Four disjoint invariant curves generated by map (22). Parameter values $P_1 = P_2 = 0.8$, $\gamma = 0$, $F = 26$. Each curve is visited once every fourth iteration. **b** Values of Lyapunov exponent. $P_1 = P_2 = 0.8$, $\gamma = 0$, $10 \le F \le 30$

Finally, the case $P_1 = P_2 = 1$ is special. Then at bifurcation threshold

$$x^* = x_F^* = x_{NS1}^* = \frac{4}{1 + 4\gamma} \qquad (29)$$

(see (25b) and (25c)) and the solutions of the eigenvalue Eq. (24) become $\lambda_1 = -1$, $\lambda_{2,3} = \pm i$, i.e. all eigenvalues are located on the boundary of the unit circle. What we observe here is that when (x_1^*, x_2^*, x_3^*) fails to be stable, the dynamics immediately turns chaotic. Such a sudden appearance of a chaotic attractor is called a crisis. There are several different mechanisms that may lead to crises, see [31–33] and references therein. The attractor we observe, and display in Fig. 11, is a result of a boundary crisis which acts as a root to chaos, cf [33].

6 Discussion

First, let us comment on survival probabilities. As shown earlier, when $n = 3$ and $1 - 2P_1 + 3P_1 P_2 < 0$ (which implies $P_1 \gg P_2$), the transfer from stability to instability does not go through a flip bifurcation but through a NS bifurcation. If the inequality is reversed the flip is the only possibility. The biological rationale behind this is as follows. When P_2 becomes small, age class 3 does not contribute in any essential way to the size of x^*. Consequently, if P_2 is small the dynamics in the 3-age class model should be retained already
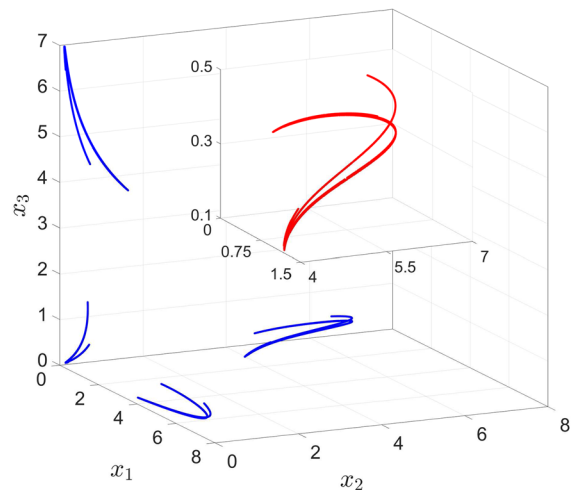

Fig. 11 A chaotic attractor (blue graph) generated by (22). $P_1 = P_2 = 1$, $\gamma = 0$ and $F = 19$. An enlarged version of the subset to the right is shown in red. Each of the (blue) subsets are visited every fourth iteration

when $n = 2$. Therefore large values of P_1 combined with P_2 small should result in quasiperiodic behaviour beyond instability threshold while P_1 and P_2 both small should lead to periodic dynamics of period 2^k. Moreover, assuming n arbitrary and $P_1, P_2, \ldots, P_{n-1}$ small one may in fact argue that the general model (3) degenerates to the one-population model ($x_1 \approx x$)

$$x_{t+1} = f(1 - \gamma x_t)^{1/\gamma} x_t \qquad (30)$$

An easy calculation shows that the equilibrium x^* of model (30) is stable as long as $x^* < 2(2\gamma+1)^{-1}$ which is the same stability criteria as we found in Theorem 1. Thus we may interpret the content of Theorem 1 as to say that $x^* < 2(2\gamma+1)^{-1}$ guarantees that $(x_1^*, \ldots, x_n^*)$ is stable in case of small survival probabilities. Since $\lambda = -1$ at threshold $x^* = 2(2\gamma+1)^{-1}$, the dynamics beyond threshold will be periodic of period 2^k. When F becomes large the dynamics turns chaotic as a result of successive flip bifurcations.

Let us now turn to the general n-age class model. As already proved (see Theorem 1) there exists a parameter region $x^* < 2/(\gamma+1)$ where the fixed point $(x_1^*, \ldots, x_n^*)$ is guaranteed to be stable. Outside this region, we have shown in our 2- and 3-age class analysis that the transfer from stability to instability may occur in different ways. If $n = 2$, the fixed point will undergo a supercritical flip bifurcation in the interval $0 < P_1 < 1/2$ and a supercritical NS bifurcation whenever $1/2 < P_1 < 1$. When $n = 3$, the region where (x_1^*, x_2^*, x_3^*) may undergo a NS bifurcation is small. In case of equal survival probabilities $P_1 = P_2 = P$, the transfer from stability to instability will always go through a flip. Now, assuming $\lambda = -1$ at threshold, the value of x^* becomes

$$x^* = \begin{cases} \dfrac{2\sum_{i=1}^{(n+1)/2} L_{2i-1}}{\sum_{i=1}^{n}(-1)^{i-1}L_i + 2\gamma\sum_{i=1}^{(n+1)/2} L_{2i-1}} & n \text{ odd} \quad (31a) \\[4mm] \dfrac{2\sum_{i=1}^{n/2} L_{2i-1}}{\sum_{i=1}^{n}(-1)^{i-1}L_i + 2\gamma\sum_{i=1}^{n/2} L_{2i-1}} & n \text{ even} \quad (31b) \end{cases}$$

and we observe that when the survival probabilities P_i, $i = 1, \ldots, n-1$ approach unity, x^* (depending on γ) tends to infinity in the even number of age classes. Consequently, we may rule out the possibility of a flip bifurcation for large survival probabilities if n is even. In Fig. 12 where $n = 4$ and $P_1 = P_2 = P_3 = P$ we show the values of x^* at bifurcation threshold. x^* is computed from

$$x^* = \frac{1 + Ka_1}{1 + (1 + Ka_1)\gamma} \tag{32}$$

where $K = \sum_{i=0}^{3} P^i$ and a_1 is defined through

$$\lambda^4 + a_1\lambda^3 + Pa_1\lambda^2 + P^2a_1\lambda + P^3a_1 = 0 \tag{33}$$

and is determined by use of the Jury criteria J_i. (A general formulation of the Jury criteria may be obtained in [34]).
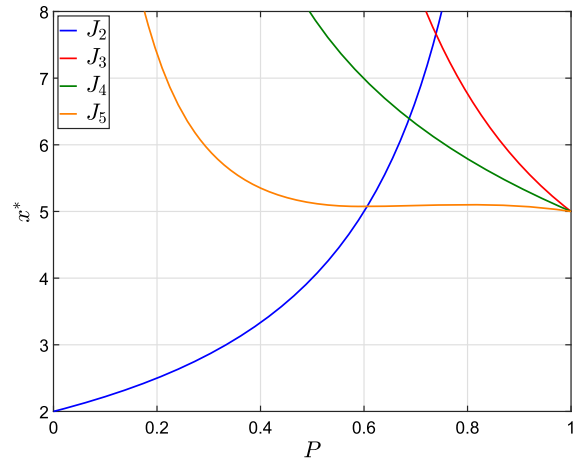

Fig. 12 Jury criteria when $n = 4$. The stable parameter region is located below the graphs

In the flip case J_2 (blue graph in Fig. 12)

$$a_1 = \frac{1}{\sum_{i=0}^{3}(-1)^i P^i}$$

In the NS cases J_3 (red graph), J_4 (green graph)

$$a_1 = \frac{1}{P^3}$$

$$a_1 = \frac{P^2 - \sqrt{P^4 - P^3(1 - P^3)}}{2P^3(1 - P^3)}$$

respectively, while a_1 in the NS case J_5 (orange graph) must be found by means of numerical methods from

$$-P^6(1 + P^4)(1 - P^2)a_1^4 - P^3(1 - 2P^2)a_1^3 + P^2(1 - 2P^4)a_1^2 - Pa_1 + 1 = 0$$

The stable parameter region is located below all graphs. In other words, if x^* is small, the fixed point $(x_1^*, x_2^*, x_3^*, x_4^*)$ will always be stable, if $P < 0.6061$ an increase of x^* (i.e. an increase of F) eventually leads to a flip bifurcation, while the fixed point will undergo a NS bifurcation if P exceeds 0.6061. Hence, we conclude that there is a great resemblance between the $n = 2$ and $n = 4$ cases. The main difference is that the P interval where a flip bifurcation may occur has been extended when $n = 4$. Moreover, when $P \to 1$ we find that a_1 in the flip case J_2 tends to infinity. In the remaining cases J_3, J_4 and J_5, $a_1 \to 1$ which proves that

$$x^* = \frac{5}{1 + 5\gamma} \tag{34}$$

at bifurcation threshold. Now, from formulas (29), (32) and (34), we find it natural to conjecture that if all survival probabilities equal unity in a general n-age class model the value of the total equilibrium population x^* at bifurcation threshold should be

$$x^* = \frac{n+1}{1 + (n+1)\gamma} \tag{35}$$

We shall now explore this further. When $P_i = 1$, $i = 1, \ldots, n-1$ then $K = n$ and the eigenvalue equation may be cast in the form

$$P(\lambda) = \lambda^n + \frac{(\gamma + 1)x^* - 1}{n(1 - \gamma x^*)}$$
$$\left(\lambda^{n-1} + \lambda^{n-2} + \cdots + \lambda + 1\right) = 0 \tag{36}$$

Further, define

$$P_0(\lambda) = \sum_{i=1}^{n} \lambda^i$$

$$P_1(\lambda) = \sum_{i=1}^{n-1} \lambda^i$$

and

$$\epsilon = \frac{(n+1) - \left(1 + (n+1)\gamma\right)x^*}{n(1 - \gamma x^*)}$$

Then, we may rewrite (36) as

$$P(\lambda) = P_0(\lambda) - \epsilon P_1(\lambda) = 0 \tag{37}$$

and if

$$\frac{n+1}{1 + (n+1)\gamma} - x^*$$

is small, ϵ is small too.

Our next goal is to show that whenever $x^* < (n+1)/(1 + [n+1]\gamma)$, i.e. $\epsilon > 0$, all eigenvalues of (37) are located on the inside of the unit circle. To this end, following the procedure outlined in [21], assume that λ_0 is a root of $P_0(\lambda) = 0$. Clearly, $\lambda_0 \neq 0$ may equal -1 if n is even, otherwise complex. Next, suppose that $\lambda = \lambda_0 + \epsilon\lambda_1 + \cdots$ is a solution of (37) when $\epsilon > 0$ and ϵ small. Then

$$\sum_{i=1}^{n} \lambda_0^i + \epsilon\lambda_1 \sum_{i=0}^{n-1}(i+1)\lambda^i - \epsilon \sum_{i=1}^{n-1}\lambda_0^{n-1} = 0$$

from which we obtain

$$\lambda_1 = -\frac{\lambda_0^n}{\sum_{i=0}^{n-1}(i+1)\lambda^i} = -\left(\frac{1}{n}\lambda_0 - \frac{1}{n}\frac{\sum_{i=1}^{n-1}i\lambda_0^i}{\sum_{i=0}^{n-1}(i+1)\lambda_0^i}\right)$$
$$= -\left(\frac{1}{n}\lambda_0 - \frac{1}{n}(1 - \lambda_1)\right)$$

which in turn implies that $\lambda_1 = (n+1)^{-1}(1 - \lambda_0)$ and

$$\lambda = \left(1 - \frac{\epsilon}{n+1}\right)\lambda_0 + \frac{\epsilon}{n+1} + O\left(\epsilon^2\right) \tag{38}$$

Finally, let $\lambda_0 = e^{i\theta}$ and consider λ_0 and λ_1 as vectors. Then

$$\bar{\lambda}_0 \cdot \epsilon\bar{\lambda}_1 = \frac{1}{2}\epsilon(\lambda_0^*\lambda_1 + \lambda_0\lambda_1^*)$$
$$= \frac{\epsilon}{n+1}(\cos\theta - 1) < 0$$

and we conclude that all eigenvalues are located on the inside of the unit circle so our conjecture is supported. x^* as defined in (35) is the bifurcation threshold when all survival probabilities equal unity. From a dynamical point of view the result above signals that in case of large survival probabilities, the region where the fixed point retains its stability will increase as n becomes larger. Hence, an increase of the number of age classes acts in a stabilizing fashion.

Next, consider an even number of age classes and equal survival probabilities. When $n = 2$ and $n = 4$ we have proved the existence of an interval $P_k < P < 1$ where the fixed point will undergo a NS bifurcation at threshold ($n = 2 \Rightarrow P_k = 0.5$, $n = 4 \Rightarrow P_k = 0.6061$). In Fig. 13 we show the value of P_k as function of n, and clearly, the larger the n, the smaller becomes the interval. However, there are limits as to how small such intervals may be. This is due to our previous finding that an increase of n (especially when P is large) acts in a stabilizing way. If P_k shall approach unity, this will only be possible in case of extreme (unrealistic) F values. Therefore, we conclude that there will always be an interval $P_k < P < 1$ where the dynamics beyond threshold consists of quasiperiodic orbits and possible chaotic dynamics.

Regarding an odd number of age classes it follows from Theorem 6 that whenever $P_1 = P_2 = P$ the flip is the only possibility when $n = 3$. Now, assume equal survival probabilities, n odd and $n \geq 3$. If the fixed point shall undergo a flip at threshold, x^* must equal (31a) from which we obtain the associated eigenvalue equation

$$\lambda^n + \frac{1}{\sum_{i=0}^{n-1}(-1)^i P^i}$$
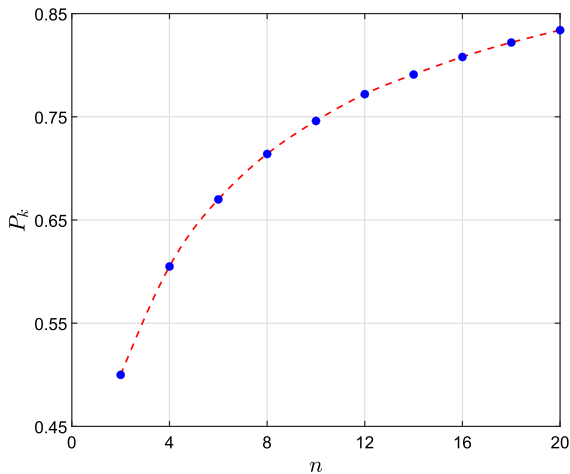$$\left(\lambda^{n-1} + P\lambda^{n-1} + \cdots + P^{n-2}\lambda + P^{n-1}\right) = 0 \tag{39}$$

Fig. 13 Values of P_k (dots) when n is even

$\lambda = -1$ is necessarily a solution of (39). The remaining solutions must be obtained from

$$\lambda^{n-1} + \frac{1}{\sum_{i=0}^{n-1}(-1)^i P^i}\left(\left(\sum_{i=1}^{n-1}(-1)^{i+1}P^i\right)\lambda^{n-2}\right.$$
$$+ \left(\sum_{i=2}^{n-1}(-1)^i P^i\right)\lambda^{n-3}$$
$$+ \left(\sum_{i=3}^{n-1}(-1)^{i+1}P^i\right)\lambda^{n-4} + \cdots$$
$$\left.+ \left(P^{n-2} - P^{n-1}\right)\lambda + P^{n-1}\right) = 0 \tag{40}$$

Applying Rouche's theorem on (40) in the same way as in the proof of Theorem 1, we find that all roots λ of (40) will satisfy $|\lambda| < 1$ if

$$\frac{P + P^3 + \cdots + P^{n-2}}{1 - P + P^2 - \cdots + P^{n-1}} < 1 \tag{41}$$

When $n = 3$, (41) is satisfied for any $0 < P \le 1$, but when n becomes large, (41) is satisfied only if $0 < P \le 1/2$. Thus $0 < P \le 1/2$ is sufficient to guarantee that there will be a flip bifurcation at threshold. However, our conjecture is that in case of any $n \ge 3$ the transfer from stability to instability will go through a flip bifurcation also when $1/2 < P < 1$. In order to support this, we have rewritten the general eigenvalue Eq. (7) under the assumption $F_1 = \cdots = F_n = F$, $P_1 = \cdots = P_{n-1} = P$ and $\alpha = 1$ as

$$\lambda^{n+1} + R\lambda^n = S \tag{42}$$

where

$$R = -\frac{P(1 - P^n) + (1 - P)(1 - x^*) - (1 - P^{n+1})\gamma x^*}{(1 - P^n)(1 - \gamma x^*)}$$

$$S = -\frac{(1 - P)P^n(1 - (\gamma + 1)x^*)}{(1 - P^n)(1 - \gamma x^*)}$$

$\lambda = P$ is one solution of (42). The others are the same as the solutions of (7). Moreover, any solution $\lambda = e^{i\theta}$ located on the boundary of the unit circle satisfies

$$\cos(n + 1)\theta + R\cos n\theta - S = 0 \tag{43a}$$
$$\sin(n + 1)\theta + R\sin n\theta = 0 \tag{43b}$$

Lots of numerical experiments show that when n is odd both equations are satisfied for the first time when $\theta = \pi$ which implies $\lambda = \cos\pi + i\sin\pi = -1$ and thus a flip bifurcation. This is exemplified in Fig. 14a where $n = 7$, $P = 0.8$ and the curves equal zero simultaneously for the first time when $x^* = 6.8795$. For comparison reasons, we have also performed similar experiments when n is even. In Fig. 14b, we show how the curves develop when $n = 8$ and $P = 0.8$. Here both curves become zero simultaneously when x^* is increased to the value $x^* = 7.8612$. Moreover, $\theta_{1,2} = \pi \pm 0.2522$ which leads to $\lambda = -0.9684 \pm 0.2495i$ with property $|\lambda| = 1$, i.e. a NS bifurcation.

7 Summary

In this paper, we have focused on nonlinear iteroparous Leslie matrix models. Nonlinearities are incorporated in fecundity terms by use of the general Deriso–Schnute recruitment function. Survival probabilities P_i are regarded as constants. Under the assumption of equal fecundities $F_1 = \cdots = F_n = F$, it is proved (Theorem 1), independent of degree of compensatory/overcompensatory recruitment (measured by parameter γ, $-1 \le \gamma < 0$), that there always exists a region where the model possesses a nontrivial stable equilibrium $(x_1^*, \ldots, x_n^*)$ and that the region becomes smaller as $\gamma \to 0$. This is in contrast to what one obtains from semelparous models where the equilibrium is unstable also at low population densities. Considering $n = 2$ age classes, it is shown that the bifurcations that occur at instability threshold (flip when $P_1 < 1/2$, NS when $1/2 < P_1 < 1$) are of supercritical
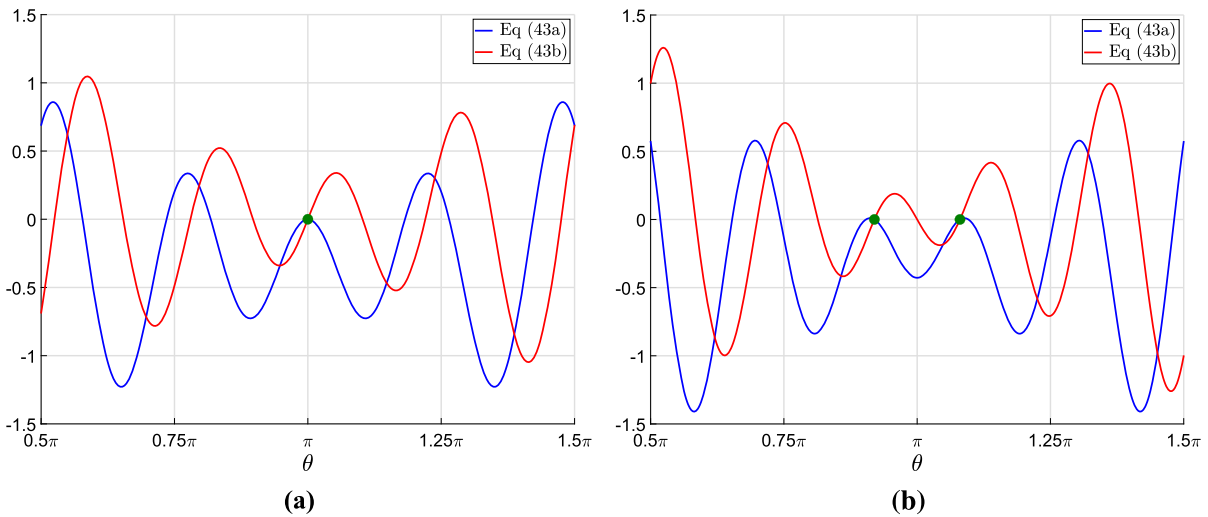
Fig. 14 Solution of Eqs. (43a) and (43b). **a** $n = 7$, $P = 0.8$. **b** $n = 8$, $P = 0.8$

nature (Theorem 2 and 4) and we also provide normal form expressions of $1 : 2$ and $1 : 3$ resonance cases (Theorem 3 and 5). Still assuming $n = 2$, we also elaborate findings about coexisting attractors. It is shown, depending on P_1, that fixed points, 2 period orbits and invariant curves may coexist with a 3-cyclic attractor with large amplitude. (In some cases the 3-cycle turns chaotic through a series of flip bifurcations which gives births to other coexistences as well). In this part of the parameter space, the ultimate fate of an orbit depends on the initial condition. A general finding is that for a fixed value of P_1 (in particular when $P_1 > 1/2$) an increase of F ($F_1 = F_2 = F$) makes the trapping region for the fixed point or the invariant curve smaller and for P_1 values close to unity the trapping region for the invariant curve consists almost exclusively of points located inside the curve.

When $n = 3$, the transfer from stability to instability goes through a supercritical flip bifurcation (Theorem 6) in most of parameter space. Hence, close to but above threshold the dynamics is 2-periodic, but in contrast to the $n = 2$ case when F is further increased there are regions where the dynamics occurs on 4 disjoint invariant curves. Moreover, in the special case $P_1 = P_2 = 1$ all eigenvalues are located on the boundary of the unit circle at instability threshold. Through further increase of F a crisis occurs and the dynamics turns instantly chaotic.

Next let us summarize our results about the dynamics when n is arbitrary. It is necessary to distinguish

between even and odd number of age classes. In the former, there exists a P ($P_1 = \cdots = P_{n-1} = P$) interval $P_k < P < 1$, $P_k > 1/2$, where the fixed point will undergo a NS bifurcation at instability threshold and as shown the interval becomes smaller as n becomes larger. Consequently, when F is sufficiently large and $P_k < P < 1$ the nonstationary dynamics just beyond instability threshold is restricted to invariant curves. On the other hand, if n is odd or $0 < P < P_k$ when n is even, periodic dynamics of period 2^k, $k \geq 1$, is the most likely outcome, but confer Fig. 10a for a counter example.

Finally, let us comment on number of age classes. Whenever P_i, $i = 2, \ldots, n - 1$, are small our findings clearly suggest that the dynamics found in a general n-age class model to a large extent will be retained already in a 2-age class model. When all survival probabilities approach unity, $x^* = x^*(n)$ at instability threshold (see (35)) is found to be an increasing function. The impact of this is that the stable parameter region expands as n is increased from which we conclude that an increase of number of age classes acts in a stabilizing fashion.

Finally, we want to stress that we have not considered any concrete species in our analysis, but what we have done, besides proving some general theorems of nature of bifurcations involved, is to show and unify results about possible dynamical outcomes in a more general setting than in previous quoted papers. Therefore, results obtained should be valuable and may con-

tribute to a better understanding of mechanisms behind observed dynamical behaviour in nature.

Declarations

Appendix A: Proof of Theorem 2

Expanding the first component of (13) up to third order about (x_1^*, x_2^*) together with the transformation $(\hat{x}_1, \hat{x}_2) = (x_1 - x_1^*, x_2 - x_2^*)$ yields at threshold

$$\hat{x}_{1,t+1} = -\frac{1}{1-P_1}\hat{x}_t + \left(f' + \frac{1}{2}f''x^*\right)\hat{x}_t^2$$
$$+ \left(\frac{1}{2}f'' + \frac{1}{6}f'''x^*\right)\hat{x}_t^3 \qquad (A.1a)$$
$$\hat{x}_{2,t+1} = P_1\hat{x}_{1,t} \qquad (A.1b)$$

where

$$f' + \frac{1}{2}f''x^* = \frac{(1+2\gamma-P_1)(P_1-\gamma)}{(1+P_1)(1-P_1)^2}$$

$$\frac{1}{2}f'' + \frac{1}{6}f'''x^*$$
$$= \frac{(1-\gamma)(1+2\gamma-P_1)^2(1+4\gamma-3P_1)}{6(1+P_1)(1-P_1)^3}$$

At threshold the eigenvalues of (10) become $\lambda_1 = -1$, $\lambda_2 = -P_1(1-P_1)$ and $|\lambda_2| < 1$. Next, define

$$T_1 = \begin{pmatrix} -\frac{1}{P_1} & -\frac{1}{1-P_1} \\ 1 & 1 \end{pmatrix} \qquad (A.2)$$

where the columns of T_1 are the associated eigenvectors of λ_1 and λ_2, respectively. Then, by use of

$$\begin{pmatrix} \hat{x}_1 \\ \hat{x}_2 \end{pmatrix} = T_1 \begin{pmatrix} u \\ v \end{pmatrix} \Leftrightarrow \begin{pmatrix} u \\ v \end{pmatrix} = T_1^{-1} \begin{pmatrix} \hat{x}_1 \\ \hat{x}_2 \end{pmatrix} \qquad (A.3)$$

we may express (A.1a) and (A.1b) as

$$\begin{pmatrix} u \\ v \end{pmatrix}_{t+1} = \begin{pmatrix} -1 & 0 \\ 0 & -\frac{P_1}{1-P_1} \end{pmatrix} \begin{pmatrix} u \\ v \end{pmatrix}_t$$
$$+ \begin{pmatrix} g(u_t, v_t) \\ -g(u_t, v_t) \end{pmatrix} \qquad (A.4)$$

where

$$g(u, v) = A\big((1-P_1)^2u + P_1^2v\big)^2$$
$$+ B\big((1-P_1)^2u + P_1^2v\big)^3$$

and

$$A = \frac{1}{P_1(2P_1-1)(1-P_1)}\left(f' + \frac{1}{2}f''x^*\right)$$
$$B = \frac{1}{P_1^2(2P_1-1)(1-P_1)^2}\left(\frac{1}{2}f'' + \frac{1}{6}f'''x^*\right)$$

Next, by use of the procedure outlined in [35] we may restrict (A.4) to the centre manifold as

$$u_{t+1} = w(u_t) = -u_t + A(1-P_1)^4u_t^2 + (1-P_1)^6$$
$$\big(B - 2A^2P_1^2(1-P_1)\big)u_t^3 \qquad (A.5)$$

Still, following [35] the bifurcation will be of supercritical nature whenever

$$\frac{\partial w}{\partial F}\frac{\partial^2 w}{\partial u^2} + 2\frac{\partial^2 w}{\partial u \partial F} \neq 0 \qquad (A.6a)$$
$$\frac{1}{2}\left(\frac{\partial^2 w}{\partial u^2}\right)^2 + \frac{1}{3}\left(\frac{\partial^3 w}{\partial u^3}\right) > 0 \qquad (A.6b)$$

The left-hand side of (A.6a) (the nondegeneracy condition) becomes

$$-2\left(\frac{2\gamma}{1-P_1} + 1\right)^{1-1/\gamma}\frac{(1-P_1)^2}{1-2P_1}$$

and is clearly nonzero while the left-hand side of (A.6b) may be expressed as

$$\left(\frac{2\gamma}{1-P_1}+1\right)^2 \frac{2(1-P_1)^3}{P_1^2(1+P_1)(1-2P_1)}$$
$$\left((P_1-\gamma)^2+\frac{1}{6}(1-\gamma)(4\gamma-3P_1+1)\right)$$

and since $\gamma > -1/2$ makes $\gamma > -(1-P_1)/2$ for all $P_1, 0 < P_1 \le 1/2$, we find that

$$(P_1-\gamma)^2+\frac{1}{6}(1-\gamma)(4\gamma-3P_1+1)$$
$$> P_1^2+\frac{1}{4}P_1 > 0$$

Consequently, the left-hand side of (A.6b) is positive and we conclude that the bifurcation is supercritical.

Appendix B: Proof of Theorem 3

When $P_1 = 1/2$, the Jacobian matrix evaluated at threshold becomes

$$J_0 = \begin{pmatrix} -2 & -2 \\ 1/2 & 0 \end{pmatrix}$$

Consequently, $\lambda_1 = \lambda_2 = -1$ and an eigenvector $\overline{u}_0$ and generalized eigenvector $\overline{u}_1$ satisfying $J_0\overline{u}_0 = -\overline{u}_0$, $J_0\overline{u}_1 = -\overline{u}_1 + \overline{u}_0$ are found to be $\overline{u}_0 = (-2, 1)^T$ and $\overline{u}_1 = (2, 0)^T$ respectively. Define the matrix $T_2 = (\overline{u}_0, \overline{u}_1)$. Then by use of

$$\begin{pmatrix} \hat{x}_1 \\ \hat{x}_2 \end{pmatrix} = T_2 \begin{pmatrix} y_1 \\ y_2 \end{pmatrix} \Leftrightarrow \begin{pmatrix} y_1 \\ y_2 \end{pmatrix} = T_2^{-1} \begin{pmatrix} \hat{x}_1 \\ \hat{x}_2 \end{pmatrix}$$

and $Q = P_1 - 1/2$, (13) may be transformed to

$$\begin{pmatrix} y_1 \\ y_2 \end{pmatrix}_{t+1} = \begin{pmatrix} -1+a(Q) & 1+b(Q) \\ c(Q) & -1+d(Q) \end{pmatrix} \begin{pmatrix} y_1 \\ y_2 \end{pmatrix}_t$$
$$+ \begin{pmatrix} g(\overline{y}_t, Q) \\ h(\overline{y}_t, Q) \end{pmatrix} \quad \text{(B.1)}$$

where $a(Q) = -2Q, b(Q) = 2Q, C(Q) = 4Q^2/(1-2Q), D(Q) = -2Q(1+2Q)/(1-2Q)$, with properties $a(0) = b(0) = c(0) = d(0) = 0$ and

$$g(\overline{y}_t, Q) = 0$$
$$h(\overline{y}_t, Q) = \frac{1}{2}\left(\frac{2(1+4\gamma-2Q)(1-2\gamma+2Q)}{(1-2Q)^2(3+2Q)}\right.$$
$$(2y_{2,t}-y_{1,t})^2 - (1-\gamma)$$

$$\frac{(1+4\gamma-2Q)^2(1-8\gamma+6Q)}{3(1-2Q)^3(3+2Q)}$$
$$\left.(2y_{2,t}-y_{1,t})^3\right)$$

Next, following the procedure outlined in Lemma 9.7 in [30], denote the matrix in Eq. (B.1) for $M(Q)$ and define

$$B(Q) = \begin{pmatrix} 1+2Q & 0 \\ 2Q & 1 \end{pmatrix}$$

Then

$$B^{-1}(Q)M(Q)B(Q) = \begin{pmatrix} -1 & 1 \\ \epsilon(Q) & -1+\delta(Q) \end{pmatrix}$$
$$= \begin{pmatrix} -1 & 1 \\ 0 & -\frac{1+2Q}{1-2Q} \end{pmatrix} \quad \text{(B.2)}$$

where

$$\epsilon(Q) = c(Q) + b(Q)c(Q) - a(Q)d(Q) = 0$$
$$\delta(Q) = a(Q) + d(Q) = -\frac{4Q}{1-2Q}$$

By use of the nonlinear coordinate transform

$$\begin{pmatrix} y_1 \\ y_2 \end{pmatrix} = B(Q) \begin{pmatrix} u_1 \\ u_2 \end{pmatrix} \quad \text{(B.3)}$$

it now follows from (B.1) and (B.2)

$$\begin{pmatrix} u_1 \\ u_2 \end{pmatrix}_{t+1} = B^{-1}(Q) \begin{pmatrix} y_{1,t+1} \\ y_{2,t+1} \end{pmatrix}$$
$$= \begin{pmatrix} -1 & 1 \\ \epsilon(Q) & -1+\delta(Q) \end{pmatrix} \begin{pmatrix} u_1 \\ u_2 \end{pmatrix}_t$$
$$+ B^{-1}(Q) \begin{pmatrix} g(B(Q)\overline{u}_t, Q) \\ h(B(Q)\overline{u}_t, Q) \end{pmatrix} \quad \text{(B.4)}$$
$$= \begin{pmatrix} -1 & 1 \\ \epsilon(Q) & -1+\delta(Q) \end{pmatrix} \begin{pmatrix} u_1 \\ u_2 \end{pmatrix}_t$$
$$+ \begin{pmatrix} G(\overline{u}_t, Q) \\ H(\overline{u}_t, Q) \end{pmatrix}$$

where $G(\overline{u}, Q) = 0$ and

$$H(\overline{u}, Q) = \frac{(1+4\gamma-2Q)(1-2\gamma+2Q)}{(1-2Q)^3(3+2Q)}$$
$$\left((2Q-1)u_1+2u_2\right)^2 - \frac{1}{6}(1-\gamma)$$
$$\frac{(1+4\gamma-2Q)^2(1-8\gamma+6Q)}{(1-2Q)^3(3+2Q)}$$
$$\left((2Q-1)u_1+2u_2\right)^3$$
$$\quad \text{(B.5)}$$

Now, let $\beta_1(Q) = \epsilon(Q)$ and $\beta_2(Q) = \delta(Q)$ with properties $\beta_1(0) = \epsilon(0) = 0$ and $\beta_2(0) = \delta(0) = 0$. Then, from (B.5)

$$
\begin{aligned}
H(\overline{u}, \overline{\beta}) &= \frac{4A}{(\beta_2 - 2)^2} u_1^2 + \frac{8A}{\beta_2 - 2} u_1 u_2 + 4A u_2^2 \\
&\quad + \frac{8B}{(\beta_2 - 2)^3} u_1^3 + \frac{24B}{(\beta_2 - 2)^2} u_1^2 u_2 \\
&\quad + \frac{24B}{\beta_2 - 2} u_1 u_2^2 + 8B u_2^3 \\
&= h_{20} u_1^2 + h_{11} u_1 u_2 + h_{02} u_2^2 + h_{30} u_1^3 \\
&\quad + h_{21} u_1^2 u_2 + h_{12} u_1 u_2^2 + h_{03} u_2^3
\end{aligned}
\tag{B.6}
$$

where

$$
A = \frac{(4\gamma(\beta_2 - 2) - 2)(2(\beta_2 - 1) - 2\gamma(\beta_2 - 2))(\beta_2 - 2)}{8(2\beta_2 - 3)}
$$

$$
B = \frac{1}{96}(1 - \gamma)\frac{(4\gamma(\beta_2 - 2) - 2)^2(2(2\beta_2 - 1) - 8\gamma(\beta_2 - 2))(\beta_2 - 2)}{2\beta_2 - 3}
$$

Finally, confer Lemma 9.9 in [30] (normal form for 1 : 2 resonance), there exists a smooth invertible coordinate transform which brings (B.4) ($\beta_1 = \epsilon(Q)$, $\beta_2 = \delta(Q)$) over to

$$
\begin{pmatrix} \xi_1 \\ \xi_2 \end{pmatrix}_{t+1} = \begin{pmatrix} -1 & 1 \\ \beta_1 & 1 + \beta_2 \end{pmatrix} \begin{pmatrix} \xi_1 \\ \xi_2 \end{pmatrix}_t \\
+ \begin{pmatrix} 0 \\ C(\beta)\xi_{1,t}^3 + D(\beta)\xi_{1,t}^2\xi_{2,t} \end{pmatrix}
\tag{B.7}
$$

where

$$
C(0) = h_{30}(0) + \frac{1}{2}h_{20}^2(0) + \frac{1}{2}h_{20}(0)h_{11}(0)
$$

$$
\begin{aligned}
D(0) &= h_{21}(0) + \frac{5}{4}h_{20}(0)h_{11}(0) + h_{20}(0)h_{02}(0) \\
&\quad + h_{20}^2(0) + \frac{1}{2}h_{11}^2(0)
\end{aligned}
$$

Thus

$$
C(0) = \frac{1}{18}(4\gamma + 1)^2(-4\gamma^2 + 3\gamma - 2)
$$

$$
D(0) = \frac{1}{9}(4\gamma + 1)^2(8\gamma^2 - 5\gamma + 5)
$$

Appendix C: Proof of Theorem 4

At threshold (19), the modulus 1 solutions of (10) become

$$
\lambda = -\frac{1}{2P_1} + \frac{b}{2P_1}i
$$

$$
\overline{\lambda} = -\frac{1}{2P_1} - \frac{b}{2P_1}i
$$

where $b = (4P_1^2 - 1)^{1/2}$. Moreover,

$$
\frac{\mathrm{d}}{\mathrm{d}F}|\lambda| = \frac{P_1}{2}\left(1 + \gamma\frac{1 + 2P_1}{P_1}\right)^{\frac{\gamma - 1}{\gamma}} > 0
$$

which implies that the eigenvalues leave the unit circle at threshold. Equations (A.1a) and (A.1b) (see Appendix A) are still valid but since (x_1^*, x_2^*) at threshold now is given by (19) we have

$$
\begin{aligned}
f' + \frac{1}{2}f''x^* &= \frac{(P_1 + \gamma(1 + 2P_1))(1 - \gamma(1 + 2P_1))}{2(1 + P_1)P_1^2} \\
&= A
\end{aligned}
\tag{C.1}
$$

and

$$
\begin{aligned}
&\frac{1}{2}f'' + \frac{1}{6}f'''x^* \\
&= -\frac{(1 - \gamma)(P_1 + \gamma(1 + 2P_1))^2(1 - P_1 - 2\gamma(1 + 2P_1))}{6(1 + P_1)P_1^3} \\
&= B
\end{aligned}
\tag{C.2}
$$

The transition matrix T_3 (confer (A.2)) which now consists of the real and imaginary parts of eigenvectors associated with λ as columns is found to be

$$
T_3 = \begin{pmatrix} -\frac{1}{2P_1^2} & -\frac{b}{2P_1^2} \\ 1 & 0 \end{pmatrix}
\tag{C.3}
$$

and by use of the transformations

$$
\begin{pmatrix} \hat{x}_1 \\ \hat{x}_2 \end{pmatrix} = T_3 \begin{pmatrix} u \\ v \end{pmatrix} \Leftrightarrow \begin{pmatrix} u \\ v \end{pmatrix} = T_3^{-1} \begin{pmatrix} \hat{x}_1 \\ \hat{x}_2 \end{pmatrix}
$$

we find (confer (A.4)) that map (13) may be written in standard form as

$$
\begin{pmatrix} u_{t+1} \\ v_{t+1} \end{pmatrix} = \begin{pmatrix} -\frac{1}{2P_1} & -\frac{b}{2P_1} \\ \frac{b}{2P_1} & -\frac{1}{2P_1} \end{pmatrix} \begin{pmatrix} u_t \\ v_t \end{pmatrix} + \begin{pmatrix} 0 \\ g(u_t, v_t) \end{pmatrix}
\tag{C.4}
$$

where

$$
\begin{aligned}
g(u, v) &= -\frac{2P_1^2 - 1}{2bP_1^2}Au^2 + \frac{2P_1^2 - 1}{P_1^2}Auv \\
&\quad - \frac{b}{2P_1^2}Av^2 - \frac{(2P_1^2 - 1)^3}{4bP_1^4}Bu^3 \\
&\quad + \frac{3(2P_1^2 - 1)^2}{4P_1^4}Bu^2v \\
&\quad - \frac{3(2P_1^2 - 1)b}{4P_1^4}Buv^2 + \frac{b^2}{4P_1^4}Bv^3
\end{aligned}
$$

Next, let $z = u + vi$ and $N = 0 + ig(u, v)$. Then we may express (C.4) in complex form as

$$
\begin{aligned}
z_{t+1} &= \lambda z_t + ig\left(\frac{z_t + \overline{z}_t}{2}, \frac{z_t - \overline{z}_t}{2i}\right) \\
&= \lambda z_t + \alpha_1 z_t^2 + \alpha_2 z_t \overline{z}_t + \alpha_3 \overline{z}_t^2 + \alpha_4 \overline{z}_t^3 \\
&\quad + \alpha_5 z_t^2 \overline{z}_t + \alpha_6 z_t \overline{z}_t^2 + \alpha_7 \overline{z}_t^3
\end{aligned}
\tag{C.5}
$$

with complex coefficients

$$
\alpha_1 = \frac{A}{8bP_1^2}\left(2b(2P_1^2 - 1) + i(b^2 - (2P_1^2 - 1)^2)\right)
$$

$$
\alpha_2 = -\frac{P_1^2}{b}Ai
$$

$$
\alpha_3 = \frac{A}{8bP_1^2}\left(-2b(2P_1^2 - 1) + i(b^2 - (2P_1^2 - 1)^2)\right)
$$

$$
\alpha_5 = \frac{3B}{8b}\left(b - i(2P_1^2 - 1)\right)
$$

The next step is to simplify (C.5). Assuming $\lambda^n \neq 1$, $n = 1, 2, 3, 4, 5$, we may by use of near-identity transformation $z = w + \beta_1 w^2 + \beta_2 w\overline{w} + \beta_3 \overline{w}^2$ and its inverse $w = z - (\beta_1 z^2 + \beta_2 z\overline{z} + \beta_3 \overline{z}^2)$ express (C.5) as

$$
\begin{aligned}
w_{t+1} &= \lambda w_t + (\lambda\beta_1 + \alpha_1 - \beta_1\overline{\lambda}^2)w_t^2 \\
&\quad + (\lambda\beta_2 + \alpha_2 - \beta_2\lambda\overline{\lambda})w_t\overline{w}_t \\
&\quad + (\lambda\beta_3 + \alpha_3 - \beta_3\overline{\lambda}^2)\overline{w}_t^2 + O(3)
\end{aligned}
\tag{C.6}
$$

and if we choose

$$
\beta_1 = \frac{\alpha_1}{\lambda^2 - \lambda}
$$

$$
\beta_2 = \frac{\alpha_2}{\lambda\overline{\lambda} - \lambda}
\tag{C.7}
$$

$$
\beta_3 = \frac{\alpha_3}{\overline{\lambda}^2 - \lambda}
$$

all second order terms of (C.6) will vanish and through two more near-identity transformations (of order 3 and 4 respectively) we may get rid of all terms of order 3 and 4 in (C.6) except the $w_t^2\overline{w}_t$ term. Thus, we obtain the normal form of (C.5)

$$
w_{t+1} = \lambda w_t + \delta w_t^2 \overline{w}_t + O(5)
\tag{C.8}
$$

where δ is the sum of α_5 and terms of first and second order which have been lifted to $w_t^2\overline{w}_t$ after the first near-identity transformation. Thus,

$$
\begin{aligned}
\delta &= \frac{(1 - 2\lambda)\overline{\lambda}}{1 - \lambda}\alpha_1\alpha_2 + \frac{1}{1 - \overline{\lambda}}\alpha_2\overline{\alpha}_2 \\
&\quad + \left(-\frac{\lambda}{1 - \lambda^3}\right)\alpha_3\overline{\alpha}_3 + \alpha_5
\end{aligned}
\tag{C.9}
$$

Moreover,

$$
\begin{aligned}
w_{t+1} &= \lambda w_t(1 + \overline{\lambda}\delta|w_t|^2) \\
&= e^{2\pi i\theta}w_t(1 + \mathrm{Re}(\overline{\lambda}\delta|w_t|^2))e^{i\,\mathrm{Im}(\overline{\lambda}\delta|w_t|^2)} \\
&\quad + O(4)
\end{aligned}
\tag{C.10}
$$

and if we introduce polar coordinates $w = re^{i\phi}$ we may express (C.10) as

$$
r_{t+1} = r_t(1 + \mathrm{Re}(\overline{\lambda}\delta)r_t^2) + O(4)
\tag{C.11a}
$$

$$
\phi_{t+1} = \phi_t + 2\pi\theta + \mathrm{Im}(\overline{\lambda}\delta)r_t^2 + O(4)
\tag{C.11b}
$$

Now, in order to obtain an attracting curve, $a = \mathrm{Re}(\overline{\lambda}\delta)$ must be negative and after multiplying (C.9) by $\overline{\lambda}$, inserting the expression for α_i from (C.5) we find

$$
\begin{aligned}
a &= -\frac{(P_1 + \gamma(1 + 2P_1))^2}{16P_1^2(1 + 2P_1)(1 + P_1)^2} \\
&\quad \Big((3P_1 + 2) + ((1 - \gamma)P_1^2 - 1)(1 + 2P_1) \\
&\quad + (\gamma^2 P_1 - \gamma(1 + 4P_1))(1 + 2P_1)^2\Big)
\end{aligned}
\tag{C.12}
$$

which is negative for $1/2 < P_1 < 1$ and $-P_1/(1 + 2\gamma) < \gamma < 0$. Consequently, the bifurcation is supercritical. Thus when (x_1^*, x_2^*) fails to be stable, an attracting invariant curve about (x_1^*, x_2^*) is established.

Appendix D: Proof of Theorem 5

When $P_1 = 1$, λ equals $-1/2 + 1/2\sqrt{3}i$, i.e. third root of unity, which implies that the denominator in the β_3 expression in (C.7) (see Appendix C) becomes zero. Hence, we cannot get rid of the $\overline{w}_t^2$ term in (C.6) so let $\beta_3 = 0$. Consequently, there will be an additional resonant term $\alpha_3\overline{w}_t^2$ in (C.8) which may be expressed as

$$
C(\gamma)\overline{w}_t^2 = -\frac{1 - 9\gamma^2}{16\sqrt{3}}(\sqrt{3} - i)\overline{w}_t^2
$$

Moreover, $\beta_3 = 0$ also implies that the $\alpha_3\overline{\alpha}_3$ in (C.9) becomes zero. Thus, when $P_1 = 1$ we find the $w_t^2\overline{w}_t$

term from (C.10) as

$$D(\gamma)w_t|w_t|^2 = \left(\frac{(1-2\lambda)\overline{\lambda}}{1-\lambda}\alpha_1\alpha_2 \right.$$
$$\left. -\frac{1}{1-\overline{\lambda}}\alpha_2\overline{\alpha}_2 + \alpha_5\right)w_t|w_t|^2$$
$$= \frac{(1+3\gamma)^2}{192}\left(9\gamma^2 + 6\gamma + 5 \right.$$
$$\left. + \sqrt{3}\gamma(3\gamma - 7)i\right)w_t|w_t|^2$$

Appendix E: Proof of Theorem 6

The proof follows the same pattern as the proof of Theorem 2. First we expand the first component of map (22) up to third order about (x_1^*, x_2^*, x_3^*) together with the transformation $(\hat{x}_1, \hat{x}_2, \hat{x}_3) = (x_1 - x_1^*, x_2 - x_2^*, x_3 - x_3^*)$ in order to bring the bifurcation to the origin. Thus, at bifurcation

$$\hat{x}_{1,t+1} = -\frac{1}{1-P_1+P_1P_2}\hat{x}_t + A\hat{x}_t^2 + B\hat{x}_t^3$$
$$\hat{x}_{2,t+1} = P_1\hat{x}_{1,t} \qquad\qquad\qquad\qquad\text{(E.1)}$$
$$\hat{x}_{3,t+1} = P_2\hat{x}_{2,t}$$

where

$$A = f' + \frac{1}{2}f''x^*$$
$$= -\frac{\left(1-P_1+P_1P_2+2\gamma(1+P_1P_2)\right)}{(1+P_1+P_1P_2)(1-P_1+P_1P_2)^2}$$
$$\cdot\left(1-P_1+P_1P_2-(1-\gamma)(1+P_1P_2)\right)$$

and

$$B = \frac{1}{2}f'' + \frac{1}{6}f'''x^*$$
$$= \frac{1}{6}(1-\gamma)\frac{\left(1-P_1+P_1P_2+2\gamma(1+P_1P_2)\right)^2}{(1+P_1+P_1P_2)(1-P_1+P_1P_2)^3}$$
$$\cdot\left(3(1-P_1+P_1P_2) - 2(1-2\gamma)(1+P_1P_2)\right)$$

The transition matrix T where the first column is the eigenvector associated with $\lambda = -1$ and the other columns are eigenvectors corresponding to

$$\lambda_{2,3} = \frac{-P_1(1-P_2) + bi}{2(1-P_1+P_1P_2)}$$

where

$$b = \sqrt{4(1-P_1+P_1P_2)P_1P_2 - P_1^2(1-P_2)^2}$$

becomes

$$T = \begin{pmatrix} \frac{1}{P_1P_2} & P_1^2(1-P_2)^2 - b^2 & \frac{(1-P_2)b}{2P_2(1-P_1+P_1P_2)^2} \\ -\frac{1}{P_2} & -\frac{P_1(1-P_2)}{2P_2(1-P_1+P_1P_2)} & -\frac{b}{2P_2(1-P_1+P_1P_2)} \\ 1 & 1 & 0 \end{pmatrix} \quad\text{(E.2)}$$

so after the transformations

$$\begin{pmatrix}\hat{x}_1 \\ \hat{x}_2 \\ \hat{x}_3\end{pmatrix} = T\begin{pmatrix}u \\ v \\ w\end{pmatrix} \Leftrightarrow \begin{pmatrix}u \\ v \\ w\end{pmatrix} = T^{-1}\begin{pmatrix}\hat{x}_1 \\ \hat{x}_2 \\ \hat{x}_3\end{pmatrix} \quad\text{(E.3)}$$

we may write map (22) in standard form as

$$\begin{pmatrix}u_{t+1} \\ v_{t+1} \\ w_{t+1}\end{pmatrix} = \begin{pmatrix} -1 & 0 & 0 \\ 0 & -\frac{P_1(1-P_2)}{2(1-P_1+P_1P_2)} & -\frac{b}{2(1-P_1+P_1P_2)} \\ 0 & \frac{b}{2(1-P_1+P_1P_2)} & -\frac{P_1(1-P_2)}{2(1-P_1+P_1P_2)} \end{pmatrix}$$
$$\begin{pmatrix}u_t \\ v_t \\ w_t\end{pmatrix} + \begin{pmatrix}b_{11}g(u_t, v_t, w_t) \\ b_{21}g(u_t, v_t, w_t) \\ b_{31}g(u_t, v_t, w_t)\end{pmatrix} \quad\text{(E.4)}$$

where

$$g(u, v, w) = A(c_1u + c_2v + c_3w)^2$$
$$+ B(c_1u + c_2v + c_3w)^3$$
$$c_1 = \frac{1-P_1+P_1P_2}{P_1P_2}$$
$$c_2 = \frac{P_1(1-P_2)\left(P_1 - 3P_2 + P_1P_2 - 2P_1P_2^2\right)}{2P_2(1-P_1+P_1P_2)^2}$$
$$c_3 = \frac{b\left(P_1(1-P_2) - P_2\right)}{2P_2(1-P_1+P_1P_2)^2}$$

and

$$b_{11} = \frac{(1-P_1+P_1P_2)P_1P_2}{1-2P_1+3P_1P_2}$$
$$b_{21} = -b_{11}$$
$$b_{31} = -\frac{(1-P_1+P_1P_2)(2-3P_1+3P_1P_2)P_1P_2}{b(1-2P_1+3P_1P2)}$$

The next step is to restrict (E.4) to the centre manifold. This is done by defining

$$\overline{m} = \begin{pmatrix}u \\ w\end{pmatrix} = \overline{f}(u) = \begin{pmatrix}a_1u^2 + b_1u^3 \\ a_2u^2 + b_2u^3\end{pmatrix} \quad\text{(E.5)}$$

and then obtain coefficients a_1, a_2, b_1, b_2 (cf the proof of Theorem 2 or the procedure outlined in [35]) from the relations

$$a_1(-u + b_{11}g)^2 + b_1(-u + b_{11}g)^3$$
$$= \left(-\frac{P_1(1-P_2)}{2(1-P_1+P_1P_2)}a_1 - \frac{b}{2(1-P_1+P_1P_2)}a_2\right)u^2$$

$$+ \left(-\frac{P_1(1-P_2)}{2(1-P_1+P_1P_2)}b_1 - \frac{b}{2(1-P_1+P_1P_2)}b_2 \right)u^3$$
$$+ b_{21}g \tag{E.6a}$$

$$a_2(-u+b_{11}g)^2 + b_2(-u+b_{11}g)^3$$
$$= \left(\frac{b}{2(1-P_1+P_1P_2)}a_1 - \frac{P_1(1-P_2)}{2(1-P_1+P_1P_2)}a_2 \right)u^2$$
$$+ \left(\frac{b}{2(1-P_1+P_1P_2)}b_1 - \frac{P_1(1-P_2)}{2(1-P_1+P_1P_2)}b_2 \right)u^3$$
$$+ b_{31}g \tag{E.6b}$$

The result becomes

$$a_1 = -A\frac{P_1(1-P_2)(1-P_1+P_1P_2)^3}{(1+P_1P_2)(1-2P_1+3P_1P_2)P_1P_2}$$

$$a_2 = -A\frac{(1-P_1+P_1P_2)^3(2+P_1^2-4P_1(1+P_1P_2)+3P_1P_2(2+P_1P_2))}{b(1+P_1P_2)(1-2P_1+3P_1P_2)P_1P_2}$$

(The values of b_1 and b_2 are of no interest since they only contribute to terms u^4 and higher). Now, substituting for v and w into the first component of (E.4) we obtain the restricted map as

$$u_{t+1} = h(u_t) = -u_t + b_{11}\Big(A\big(c_1^2 u_t^2$$
$$+ 2c_1(c_2a_1 + c_3a_2)u_t^3\big) + Bc_1^3 u_t^3 \Big) + O(4) \tag{E.7}$$

Finally, referring to the same theorem as we did in the proof of Theorem 2, the flip bifurcation will be of supercritical nature whenever

$$2b_{11}c_1\big(A^2 b_{11}c_1^3 + 2A(c_2a_1 + c_3a_2) + Bc_1^2 \big)$$
$$> 0 \tag{E.8}$$

which after substitutions and simplifications may be expressed as

$$\frac{(1-P_1+P_1P_2)\big(1-P_1+P_1P_2+2\gamma(1+P_1P_2)\big)^2}{3P_1^2 P_2^2(1+P_1P_2)(1+P_1+P_1P_2)(1-2P_1+3P_1P_2)}Q > 0 \tag{E.9}$$

where

$$Q = 2\gamma^2(1+P_1P_2)^2$$
$$+ \gamma\big[3(1+P_1P_2)^2 - 9P_1(1+P_1P_2)\big]$$
$$+ (1+P_1P_2)^2 - 3P_1(1-2P_1+P_1P_2)$$

Now, regarding the fraction in (E.9) all terms are positive. Moreover, when $P_2 > (2P_1-1)(3P_1)^{-1}$ the $[\circ]$ in Q becomes negative (negative for $P_1 > 2/7$ actually) and finally since $(1+P_1P_2)^2 - 3P_1(1-2P_1+P_1P_2)$ is positive for $P_2 > (2P_1-1)(3P_1)^{-1}$ too we conclude that the flip is supercritical.

Comment: If $P_1 = P_2 = P$ we find in the Ricker case ($\gamma \to 0$) that (E.9) may be expressed as

$$\frac{(1-P+P^2)^3[1-3P+8P^2-3P^3+P^4]}{3P^4(1+P^2)(1+P+P^2)\{1-2P+3P^2\}} > 0$$

and since the zeros of both $[\circ]$ and $\{\circ\}$ parenthesis are complex numbers the result follows immediately.

References

1. Levin, S.A., Goodyear, C.P.: Analysis of an age-structured fishery model. J. Math. Biol. **9**(3), 245–274 (1980)
2. Wikan, A.: Dynamic consequences of reproductive delay in Leslie matrix models with nonlinear survival probabilities. Math. Biosci. **146**(1), 37–62 (1997)
3. Wikan, A.: Age or stage structure? A comparison of dynamic outcomes from discrete age- and stage-structured population models. Bull. Math. Biol. **74**, 1354–1378 (2012)
4. Davydova, N.V., Diekmann, O., van Gils, S.A.: Year class coexistence or competitative exclusion for strict biennials. J. Math. Biol. **46**(2), 95–131 (2003)
5. Mjølhus, E., Wikan, A., Solberg, T.: On synchronization in semelparous populations. J. Math. Biol. **50**(1), 1–21 (2005)
6. Kon, R.: Nonexistence of synchronous orbits and class coexistence in matrix population models. SIAM J. Appl. Math. **66**(2), 616–626 (2005)
7. Cushing, J.M.: Nonlinear semelparous Leslie models. Math. Biosci. Eng. **3**(1), 17–36 (2006). (**PMID: 20361805**)
8. Cushing, J.M.: Three stage semelparous Leslie models. J. Math. Biol. **59**(1), 75–104 (2009)
9. Cushing, J.M., Henson, S.M.: Stable bifurcations in semelparous Leslie models. J. Biol. Dyn. **6**(2), 80–102 (2012)
10. Chow, Y., Kon, R.: Global dynamics of a special class of nonlinear semelparous Leslie matrix models. J. Differ. Equ. Appl. **26**, 625–642 (2020)
11. Kon, R.: Bifurcations of cycles in nonlinear semelparous Leslie matrix models. J. Math. Biol. **80**, 1187–1207 (2020)
12. Cushing, J.M.: A strong ergodic theorem for some nonlinear matrix models for the dynamics of structured populations. Nat. Resour. Model. **3**(3), 331–357 (1989)
13. Crowe, K.M.: A nonlinear ergodic theorem for discrete systems. J. Math. Biol. **32**(3), 179–191 (1994)
14. Behncke, H.: Periodical cicadas. J. Math. Biol. **40**(5), 413–431 (2000)
15. Diekmann, O., Planqué, R.: The winner takes it all: how semelparous insects can become periodical. J. Math. Biol. **80**, 283–301 (2020)
16. DeAngelis, D.L., Svoboda, L.J., Christensen, S.W., Vaughan, D.S.: Stability and return times of Leslie matrices with density-dependent survival: applications to fish populations. Ecol. Model. **8**, 149–163 (1980)
17. Bergh, M., Getz, W.: Stability of discrete age-structured and aggregated delay-difference population models. J. Math. Biol. **26**, 551–581 (1988)
18. Silva, J.A.L., Hallam, T.: Compensation and stability in nonlinear matrix models. Math. Biosci. **110**, 67–101 (1992)
19. Guckenheimer, J., Oster, G., Ipaktchi, A.: The dynamics of density dependent population models. J. Math. Biol. **4**(2), 101–147 (1977)

20. Silva, J.A.L., Hallam, T.: Effects of delay, truncation and density dependence in reproduction schedules on stability of nonlinear Leslie matrix models. J. Math. Biol. **31**(4), 367–395 (1993)

21. Wikan, A., Mjølhus, E.: Overcompensatory recruitment and generation delay in discrete age-structured population models. J. Math. Biol. **35**(2), 195–239 (1996)

22. Ugarcovici, I., Weiss, H.: Chaotic dynamics of a nonlinear density dependent population model. Nonlinearity **17**(5), 1689–1711 (2004)

23. Pickmann-Soto, H., Arela-Pérez, S., Nina, H., Valero, E.: Inverse maximal eigenvalues problems for Leslie and doubly Leslie matrices. Linear Algebra Appl. **592**, 93–112 (2020)

24. Vindenes, Y., Le Coeur, C., Caswell, H.: Introduction to matrix population models. In: Salguero-Gomez, R., Gamelon, M. (eds.) Demographic Methods Across the Tree of Life, chapter 9, pp. 163–180. Oxford University Press, Oxford (2021)

25. Rand, T., Richmond, C., Dougherty, E.: Modeling the combined impacts of host plant resistance and biological control on the population dynamics of a major pest of wheat. Pest Manag. Sci. **76** (2020)

26. Feng, C.Y., Ross, J.P., Mauger, D., Dreslik, M.J.: A long-term demographic analysis of spotted turtles (*Clemmys guttata*) in illinois using matrix models. Diversity **11**(12) (2019)

27. Khan, A.Q., Alsulami, I.M.: Discrete Leslie's model with bifurcations and control. AIMS Math. **8**(10), 22483–22506 (2023)

28. Mo, T., Thorstad, E., Sandlund, O., Berntsen, H., Fiske, P., Uglem, I.: The pink salmon invasion: a Norwegian perspective. J. Fish Biol. **93**, 06 (2018)

29. Vindstad, O.P.L., Jepsen, J.U., Molvig, H., Ims, R.A.: A pioneering pest: the winter moth (*Operophtera brumata*) is expanding its outbreak range into Low Arctic shrub tundra. Arctic Sci. **8**(2), 450–470 (2022)

30. Kuznetsov, Y.A.: Elements of applied bifurcation theory. In: Applied Mathematical Sciences, 3rd edn. Springer, New York (2004)

31. Grebogi, C., Ott, E., Yorke, J.A.: Crises, sudden changes in chaotic attractors, and transient chaos. Physica D **7**(1), 181–200 (1983)

32. Grebogi, C., Ott, E., Yorke, J.A.: Chaos, strange attractors, and fractal basin boundaries in nonlinear dynamics. Science **238**(4827), 632–638 (1987)

33. Ott, E.: Chaos in Dynamical Systems (2 edn). Cambridge University Press (2002). Section 8.3

34. Murray, J.D.: Mathematical biology. In: Biomathematics, 2nd edn. Springer, Berlin (1993)

35. Guckenheimer, J., Holmes, P.: Nonlinear oscillations, dynamical systems, and bifurcations of vector fields. In: Applied Mathematical Sciences. Springer, New York (2002)